Numerical modeling of crystal properties: from photonic crystals to monocrystalline silicon.

Vasily Zabelin

STR Group Ltd., Saint-Petersburg, Russia

Vasily.Zabelin@gmail.com

Numerical investigations of two-dimensional photonic crystal optical properties

- *Introduction: electromagnetic waves and photonic crystals.*
- *Theoretical description of two-dimensional photonic crystals.*
- *Discontinuities of the permittivity distribution. Gibbs phenomenon.*
- *Optical properties of two-dimensional photonic crystals.*
- *The effect of vertical light confinement in planar waveguides. The Guided Modes Expansion method.*
- *Analysis of the optical properties sensitivity on small variations of photonic crystal parameters.*

Distributed Bragg reflection

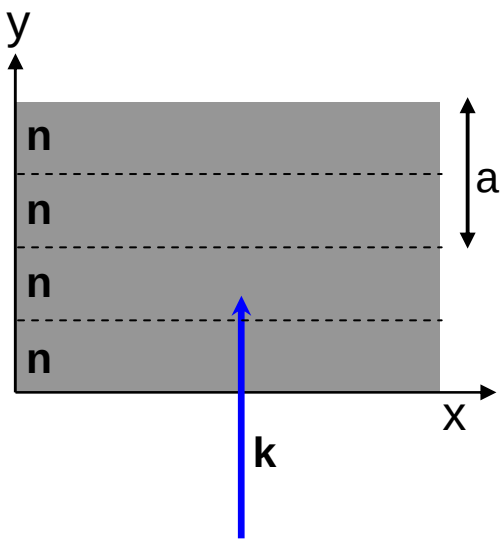

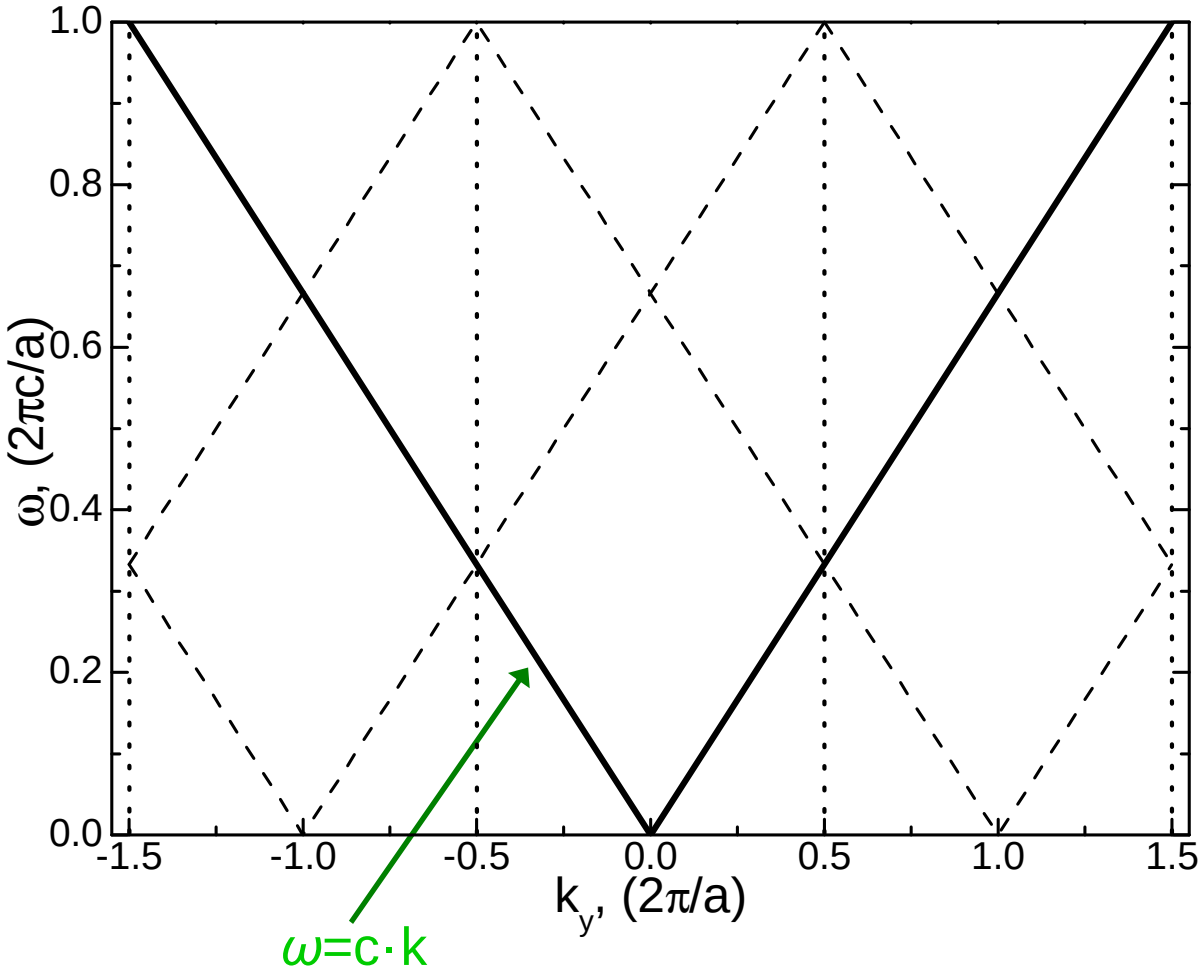

Distributed Bragg reflection

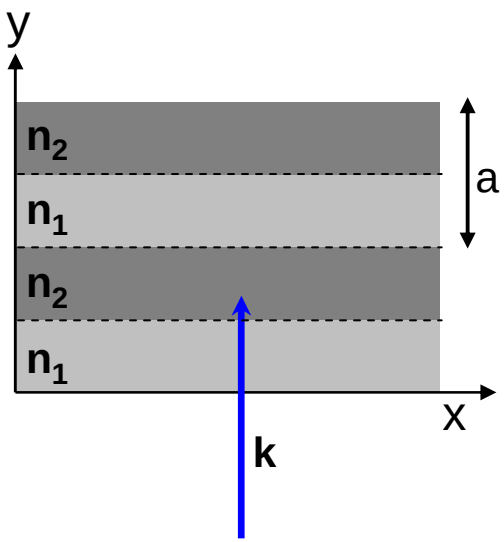

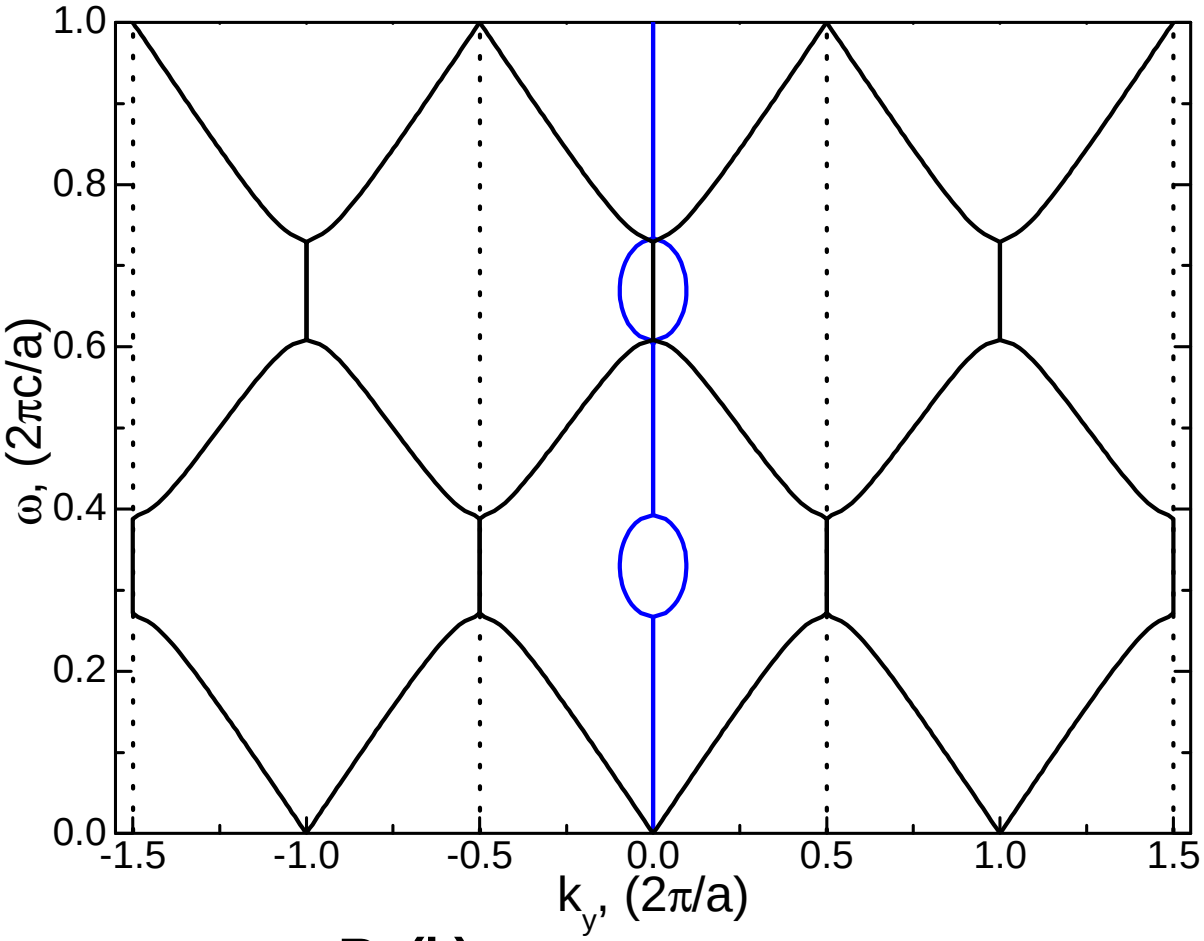

Interference of scattered light

Diffraction grating

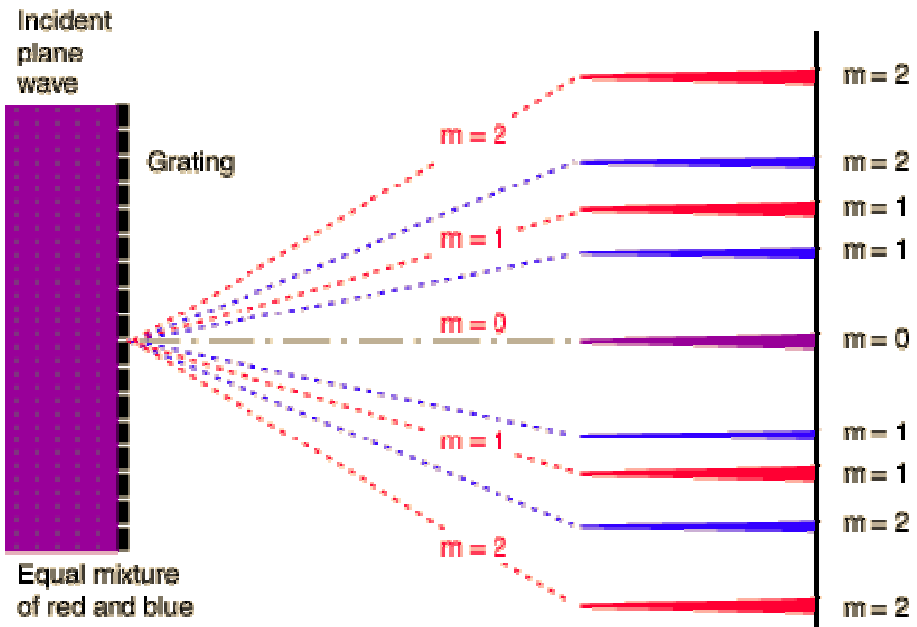

Distributed diffraction grating

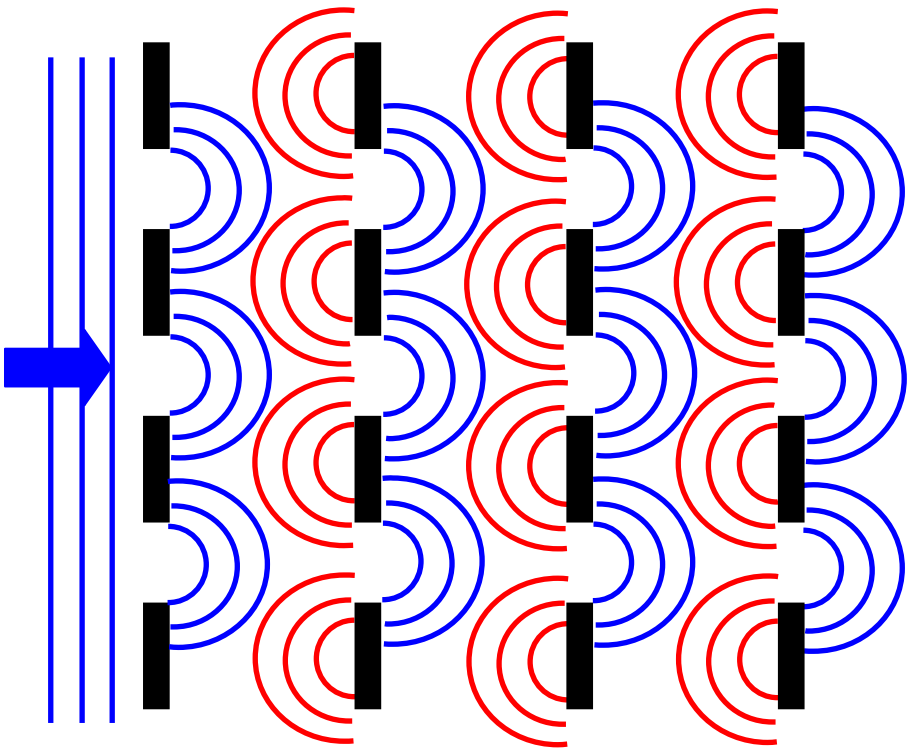

Natural photonic crystals: opals

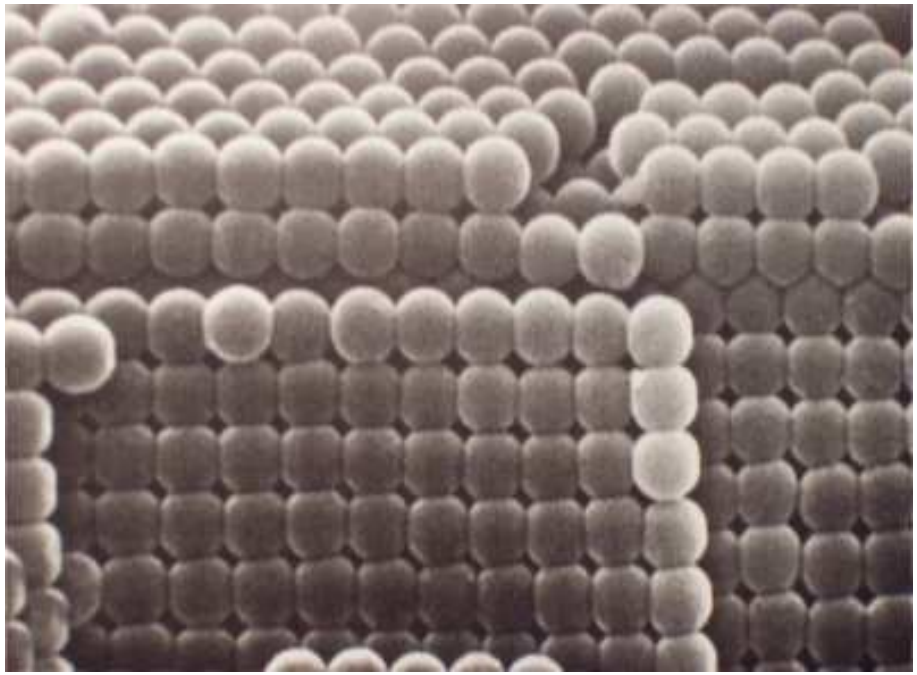

Scanning electron micrograph showing silica sphere structure of precious opal under 40000 x magnification

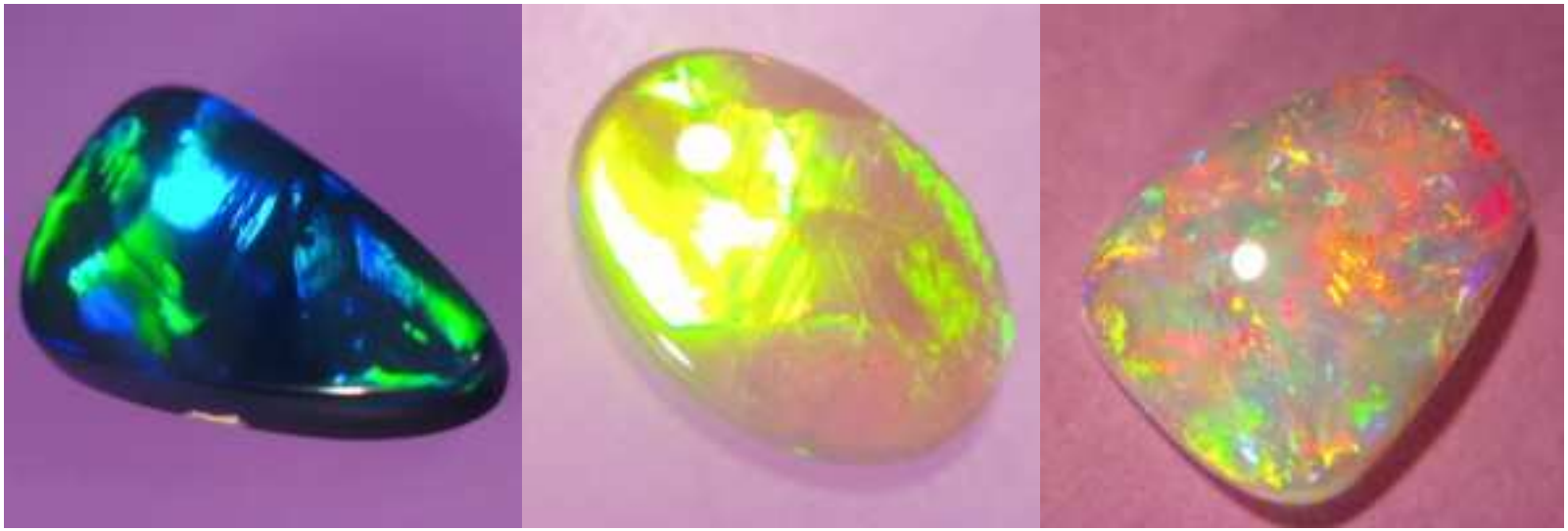

Examples of three-dimensional photonic crystals

Yablonovite

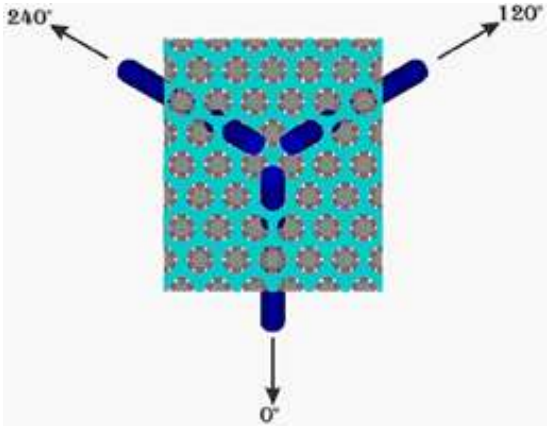

http://www.ee.ucla.edu/labs/photon/

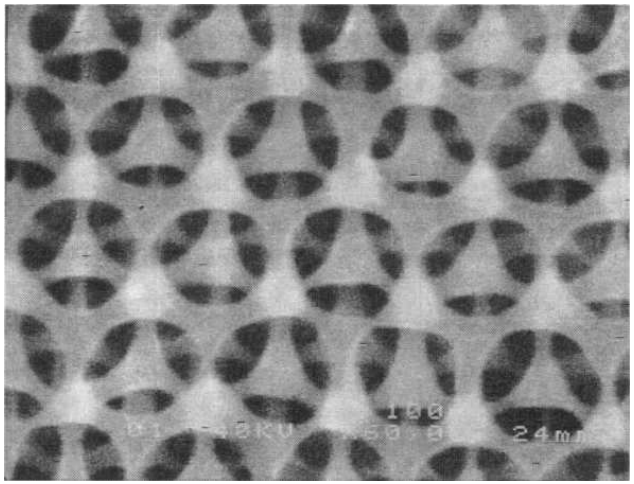

C. C. Cheng et al., Physica Scripta. T68, 17 (1996)

Woodpile structure

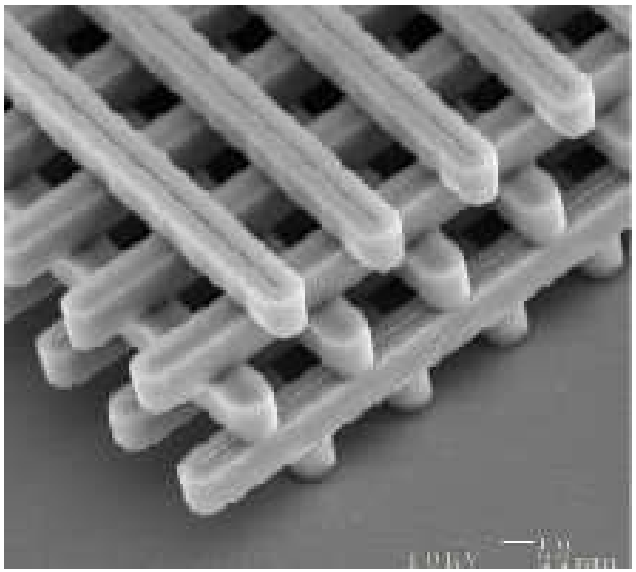

http://www.sandia.gov/media/photonic.htm

Opals and inverted opals

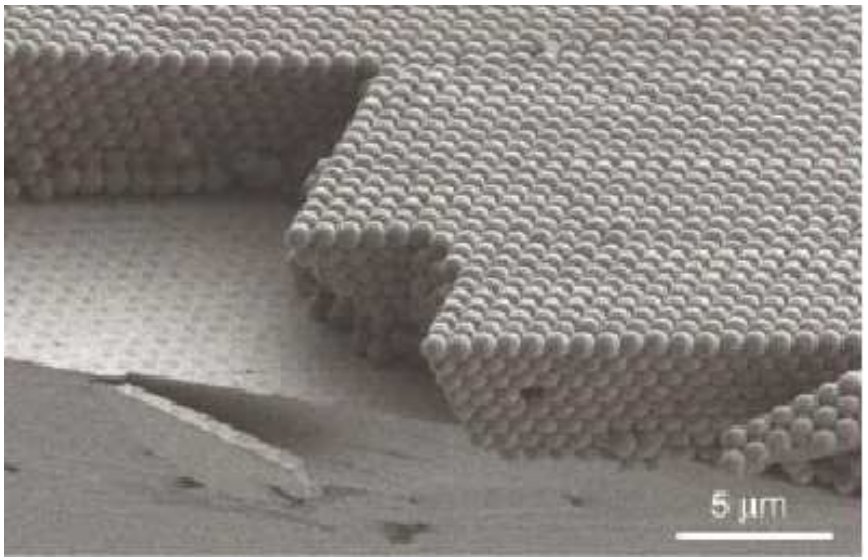

Y.A. Vlasov et al., Nature v.414 (2001)

Two-dimensional photonic crystals

Light localization in the z direction due to a planar waveguide

Periodic variation of the dielectric permittivity in the (xy) plane

$\varepsilon_v(z)$ *1D + 2D ≈ 3D* $\varepsilon_h(x,y)$

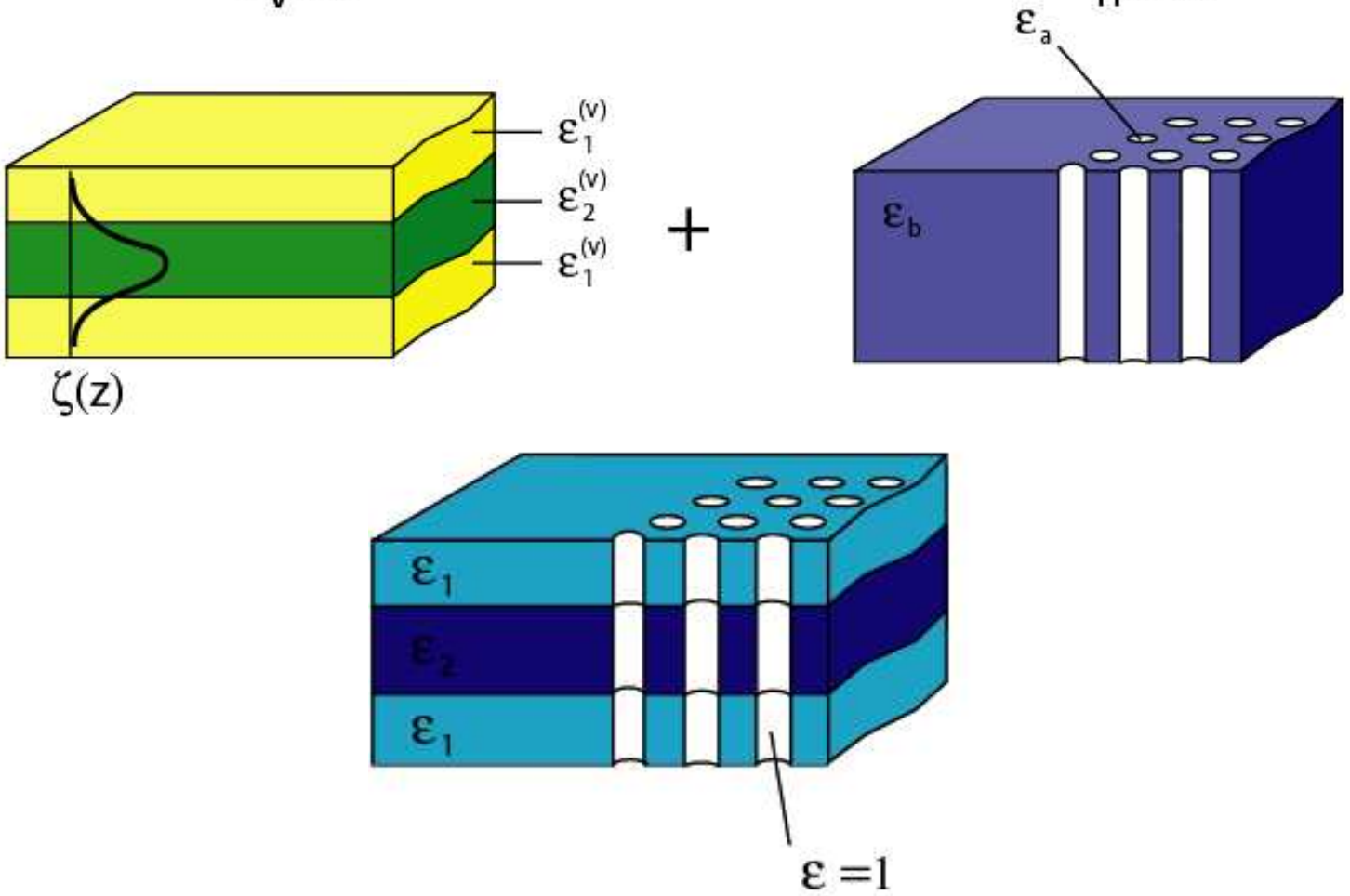

Two-dimensional photonic crystals

Etching through a slab waveguide

Holes

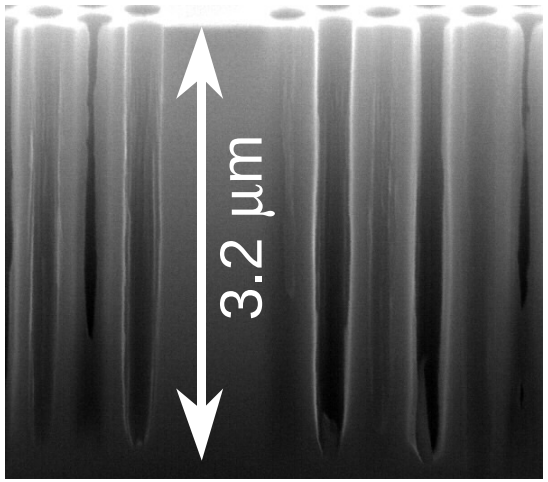

Pillars

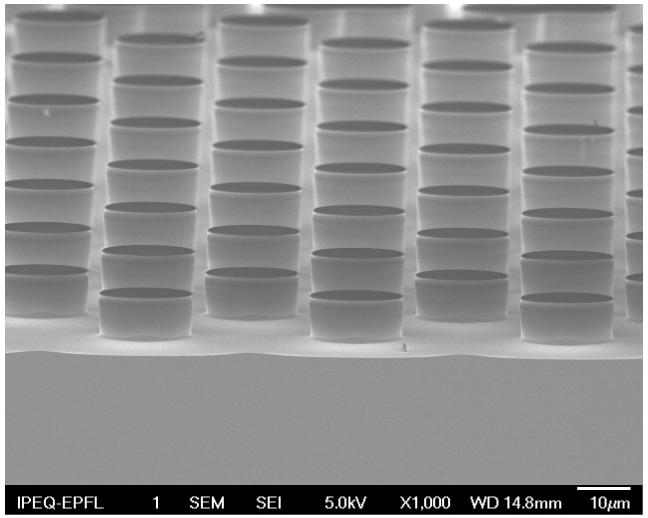

SOI

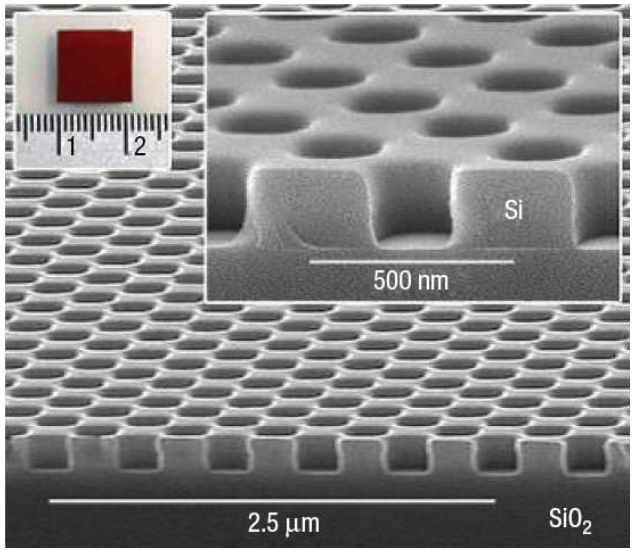

Membrane

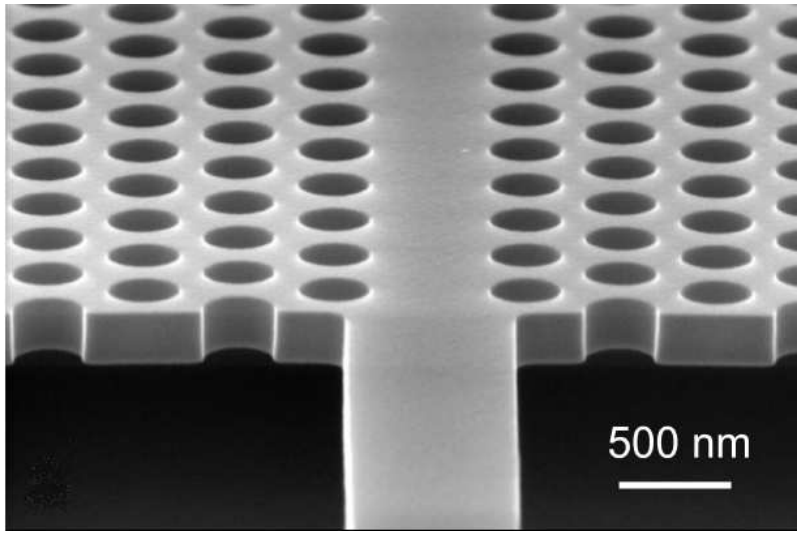

P.T. Rakich et al., Nature Materials v.5 (2006)

S.J. McNab et al., Opt. Express v.11 n.22 (2003)

Two-dimensional photonic crystals

Superprism effect

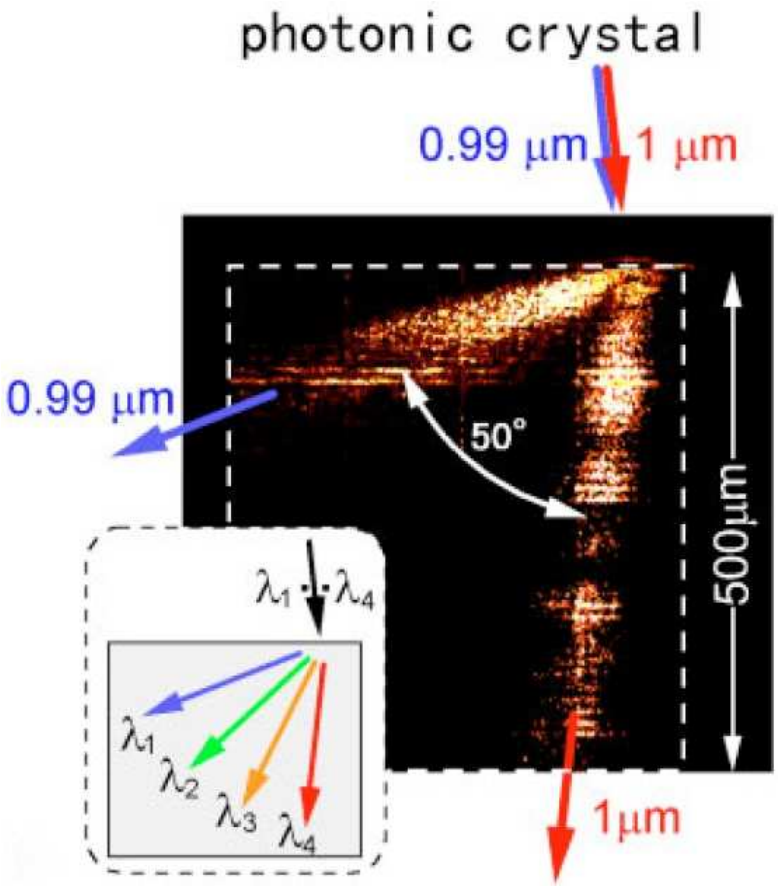

H. Kosaka et al,. APL v.74 n.10 (1999)

Self-collimation effect

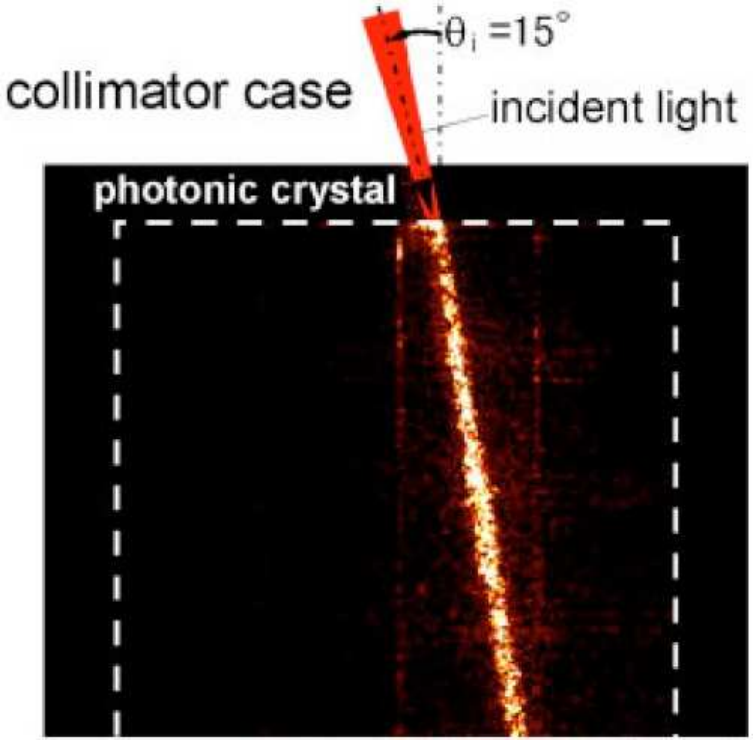

H. Kosaka et al,. APL v.74 n.9 (1999)

Two-dimensional photonic crystals

Light localization in a cavity

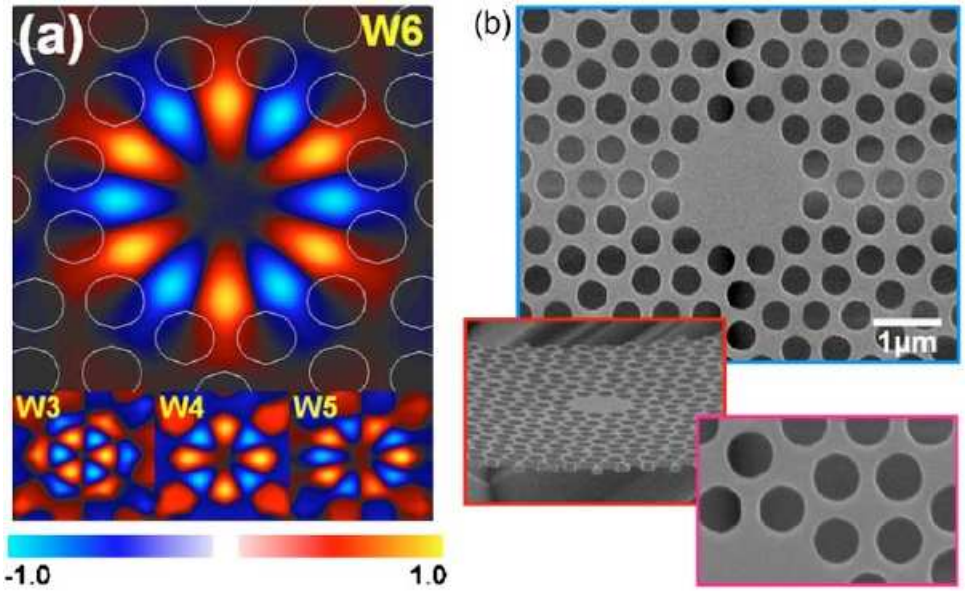

P.-T. Lee, APL v.89 (2006)

PhC waveguide

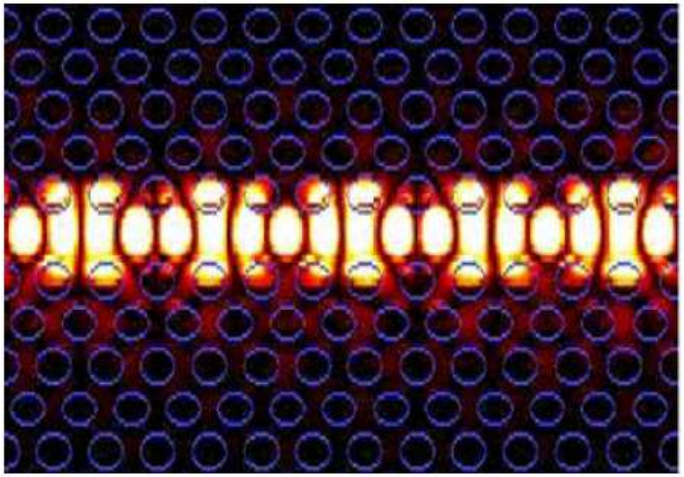

A.V. Lavrinenko et al., Appl. Phys. B v.87 (2007)

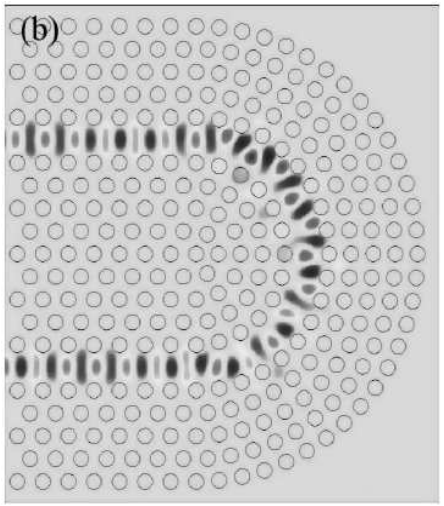

S. Xiao et al., Phys. Lett. A v.340 (2005)

Two-dimensional photonic crystals

Slow light regime in the photonic crystal waveguides

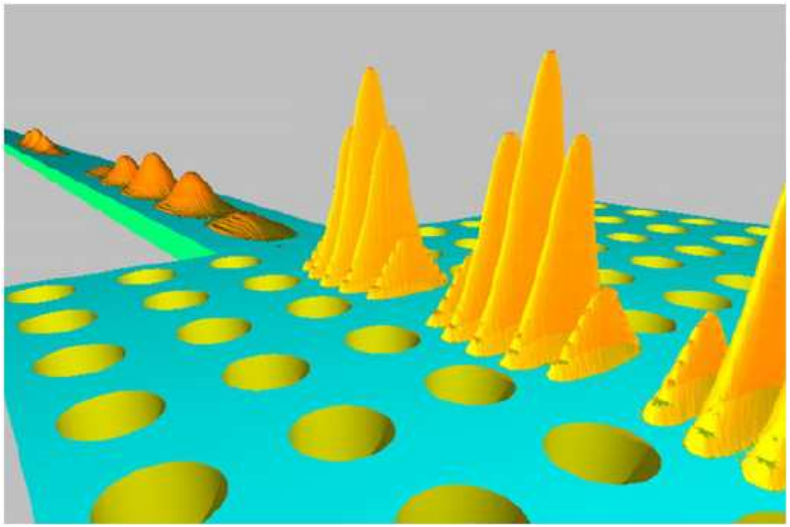

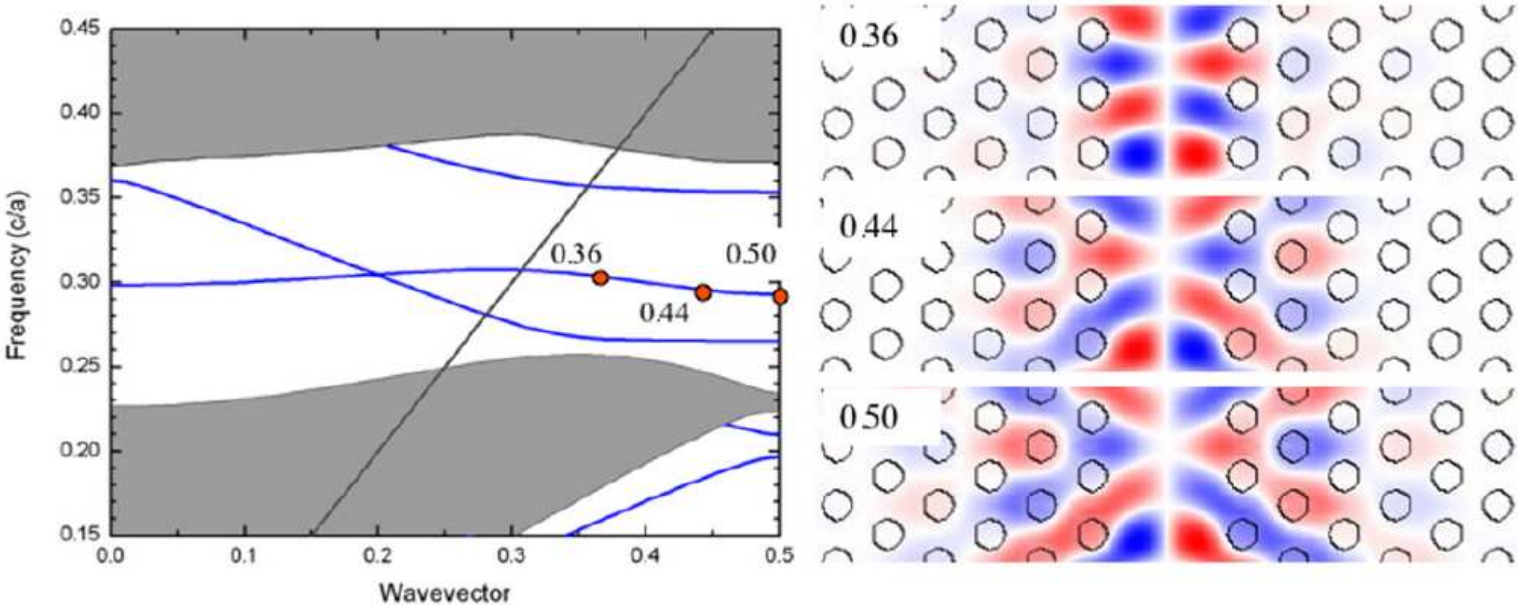

T.F. Krauss, J. Phys. D: Appl. Phys. v.40 (2007)

Numerical modelling of photonic crystal structures

Mode Expansion Methods (MEM)

The methods can handle periodic and quasi-periodic structures and calculate the dispersion relation and mode field distribution. Give details about the intrinsic properties of light states in photonic crystals.

Transfer Matrix Method / Scattering Matrix Method (TMM/SMM)

The methods can treat periodic and non-periodic structures and calculate the dispersion relation, mode field distribution, and reflection/transmission coefficient of a structure.

Finite Difference Time Domain (FDTD)

A “brute force” method which can be used to calculate light evolution in almost any structure, periodic or not, and provides direct information about the electromagnetic field distribution.

Basic properties of the photonic crystals

Maxwell's equation for the monochromatic electric **(E)** *and the monochromatic magnetic* **(H)** *fields can be written in the operator form:*

$$\mathcal{V}\mathbf{E}(\mathbf{r}) = \frac{\omega^2}{c^2}\mathbf{E}(\mathbf{r}), \text{ where } \mathcal{V} = \frac{1}{\varepsilon(\mathbf{r})}\nabla\times\frac{1}{\mu(\mathbf{r})}\nabla\times$$

$$\mathcal{W}\mathbf{H}(\mathbf{r}) = \frac{\omega^2}{c^2}\mathbf{H}(\mathbf{r}), \text{ where } \mathcal{W} = \frac{1}{\mu(\mathbf{r})}\nabla\times\frac{1}{\varepsilon(\mathbf{r})}\nabla\times$$

$$\Rightarrow \quad \mathcal{L}\psi(\mathbf{r}) = \alpha\psi(\mathbf{r})$$

The Bloch theorem

Periodicity of the dielectric permittivity and the magnetic permeability leads to the periodicity of the light state field distribution

$$\begin{cases} \varepsilon(\mathbf{r}) = \varepsilon(\mathbf{r}+\mathbf{R}) \\ \mu(\mathbf{r}) = \mu(\mathbf{r}+\mathbf{R}) \end{cases} \quad \Rightarrow \quad \mathcal{L}(\mathbf{r}) = \mathcal{L}(\mathbf{r}+\mathbf{R})$$

The Bloch state

$$\psi(\mathbf{k},\mathbf{r}) = e^{i\mathbf{k}\mathbf{r}}\varphi_{\mathbf{k}}(\mathbf{r})$$

Two-dimensional crystal lattice

Square lattice

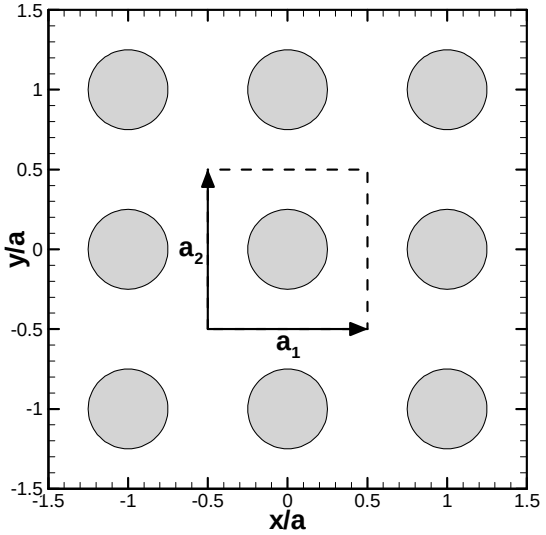

Triangular lattice

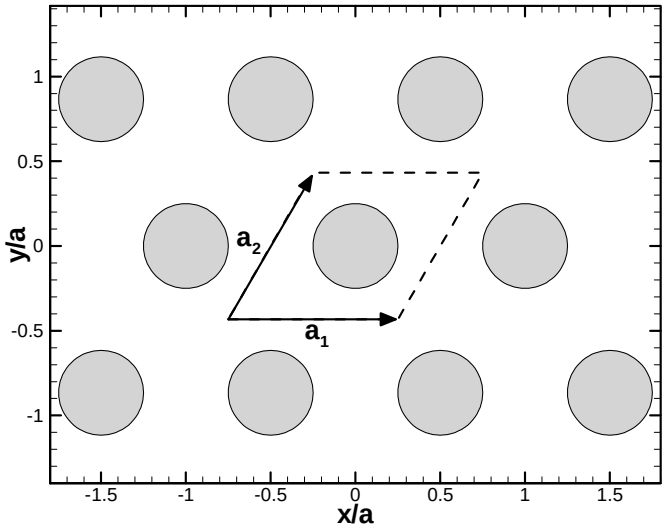

Reciprocal lattice

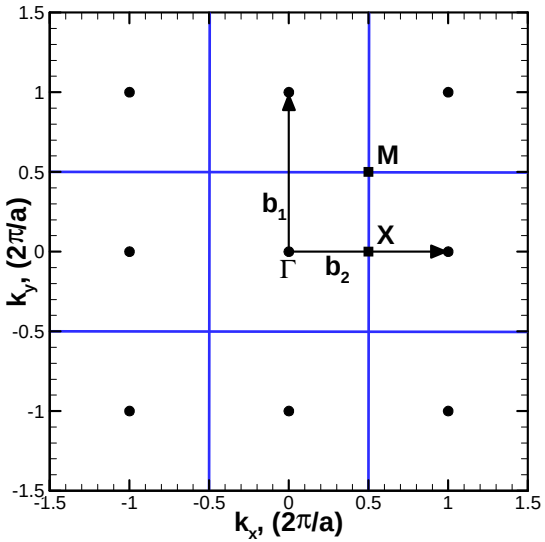

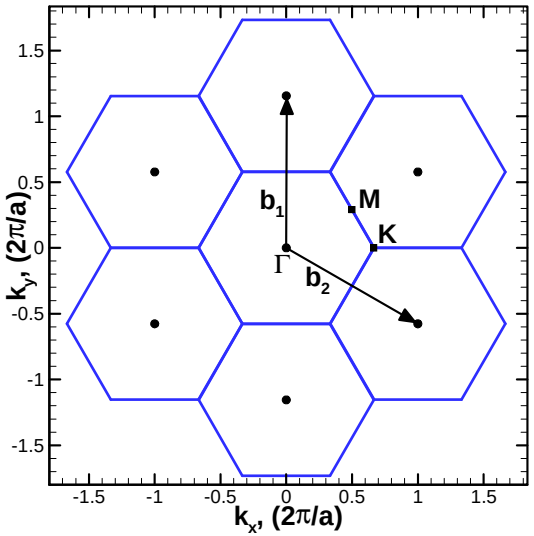

Light polarization in 2D photonic crystals

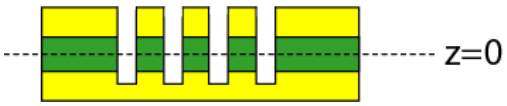

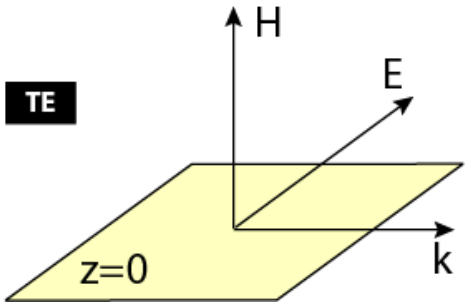

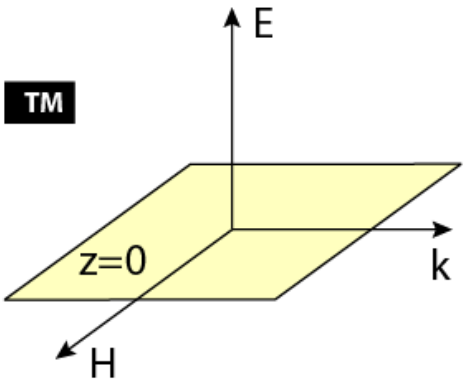

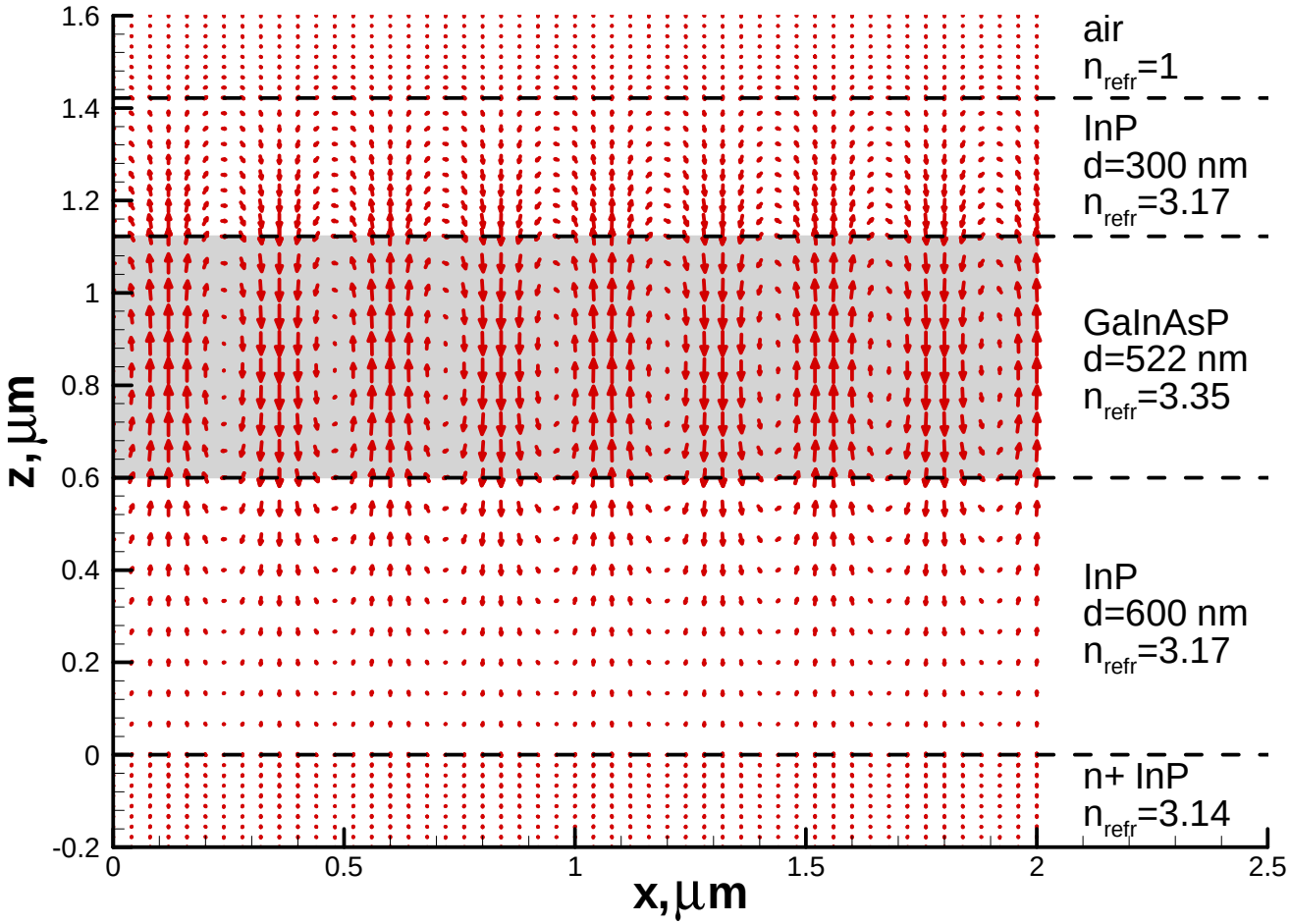

Magnetic field distribution $\mathbf{H}_{xz}$ *for the quasi-TE light polarization.* λ*=1.55* μ*m.*

The Plane Wave Expansion method

Components of the electromagnetic field are decomposed using the plane waves:

$$E_z(\mathbf{k},\mathbf{r}) = e^{i\mathbf{k}\mathbf{r}} \sum_m A_m e^{i\mathbf{G}_m\mathbf{r}} = \sum_m A_m e^{i(\mathbf{k}+\mathbf{G}_m)\mathbf{r}}$$ TM polarization

$$H_z(\mathbf{k},\mathbf{r}) = e^{i\mathbf{k}\mathbf{r}} \sum_m B_m e^{i\mathbf{G}_m\mathbf{r}} = \sum_m B_m e^{i(\mathbf{k}+\mathbf{G}_m)\mathbf{r}}$$ TE polarization

as well as the dielectric permittivity and the magnetic permeability:

$$\varepsilon(\mathbf{r}) = \sum_m \varepsilon_m e^{i\mathbf{G}_m\mathbf{r}} \qquad \frac{1}{\varepsilon(\mathbf{r})} = \sum_m \theta_m e^{i\mathbf{G}_m\mathbf{r}}$$

$$\mu(\mathbf{r}) = \sum_m \mu_m e^{i\mathbf{G}_m\mathbf{r}} \qquad \frac{1}{\mu(\mathbf{r})} = \sum_m \eta_m e^{i\mathbf{G}_m\mathbf{r}}$$

The matrix form of the governing equations:

$$\sum_n A_n \cdot \left[(\mathbf{k}+\mathbf{G}_n)\cdot(\mathbf{k}+\mathbf{G}_n)\right]\cdot\theta_{m-n} = \frac{\omega^2}{c^2} A_m$$ TM polarization

$$\sum_n B_n \cdot \left[(\mathbf{k}+\mathbf{G}_m)\cdot(\mathbf{k}+\mathbf{G}_n)\right]\cdot\theta_{m-n} = \frac{\omega^2}{c^2} B_m$$ TE polarization

The Gibbs phenomenon

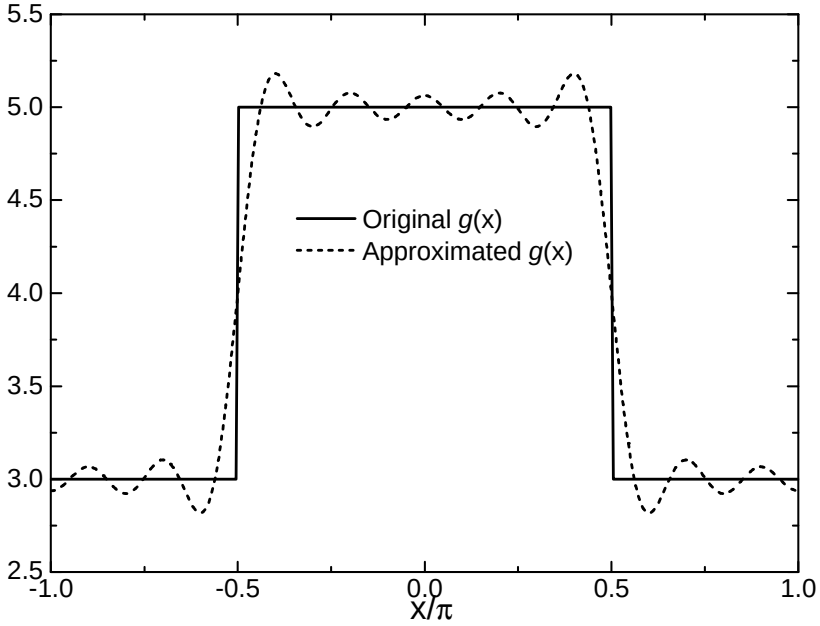

The Gibbs phenomenon leads to the oscillations of the approximated function due to the discontinuities of the original function

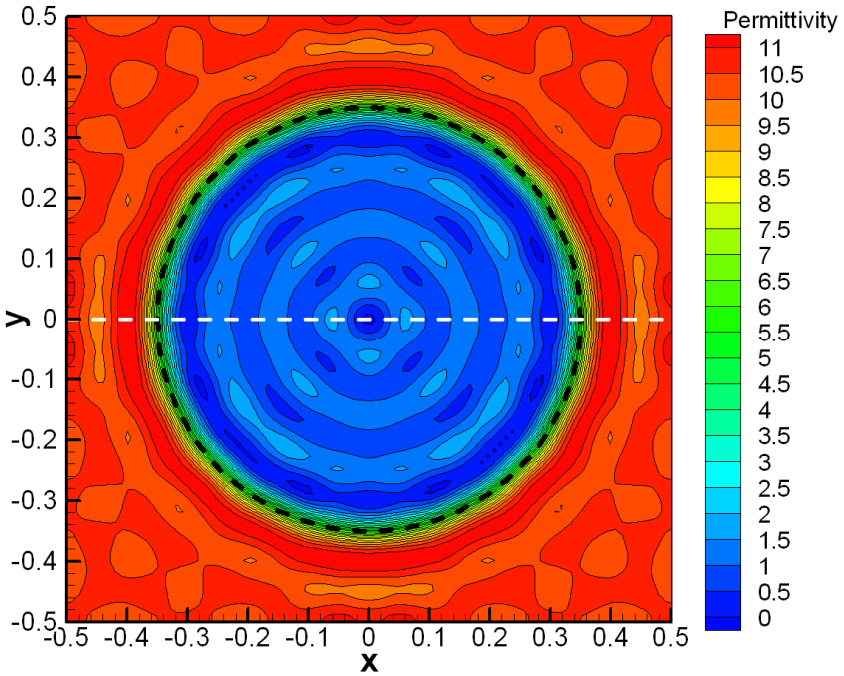

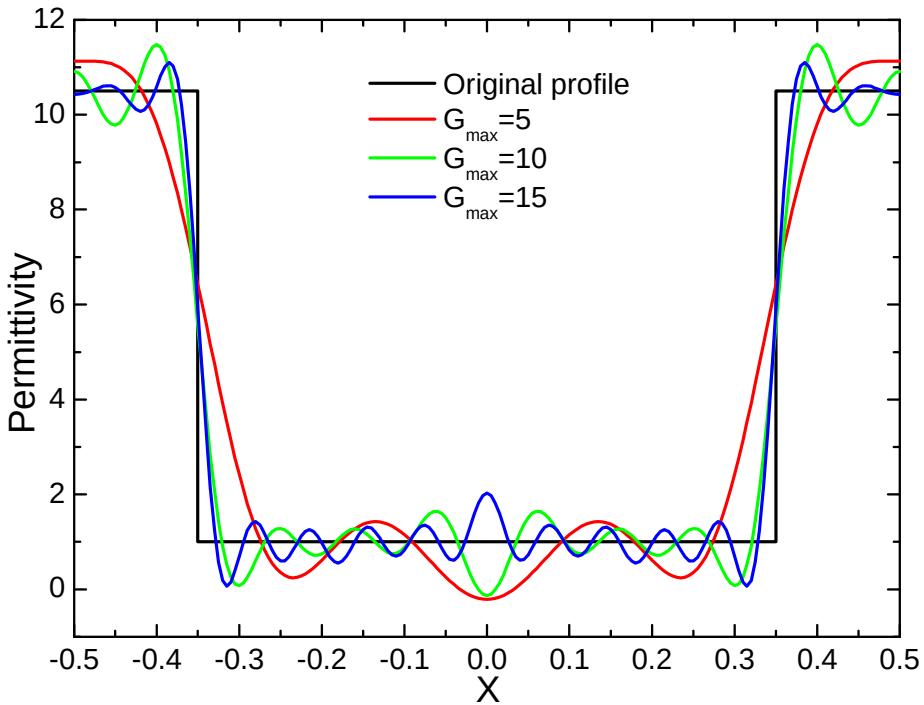

Filtering of the Gibbs phenomenon

Approximation of a periodic function using the Fourier series

$$g(x) = \sum_{n=-N}^{N} g_n e^{inx}$$

Utilization of the filter function

$$\tilde{g}(x) = \sum_{n=-N}^{N} f(n/N) g_n e^{inx}$$

Examples of the filter functions

$$f_1(t) = \frac{\sin(\pi t)}{\pi t}$$ *Lanczos filter*

$$f_2(t) = \frac{\cos(\pi t)+1}{2}$$ *Rising cosine filter*

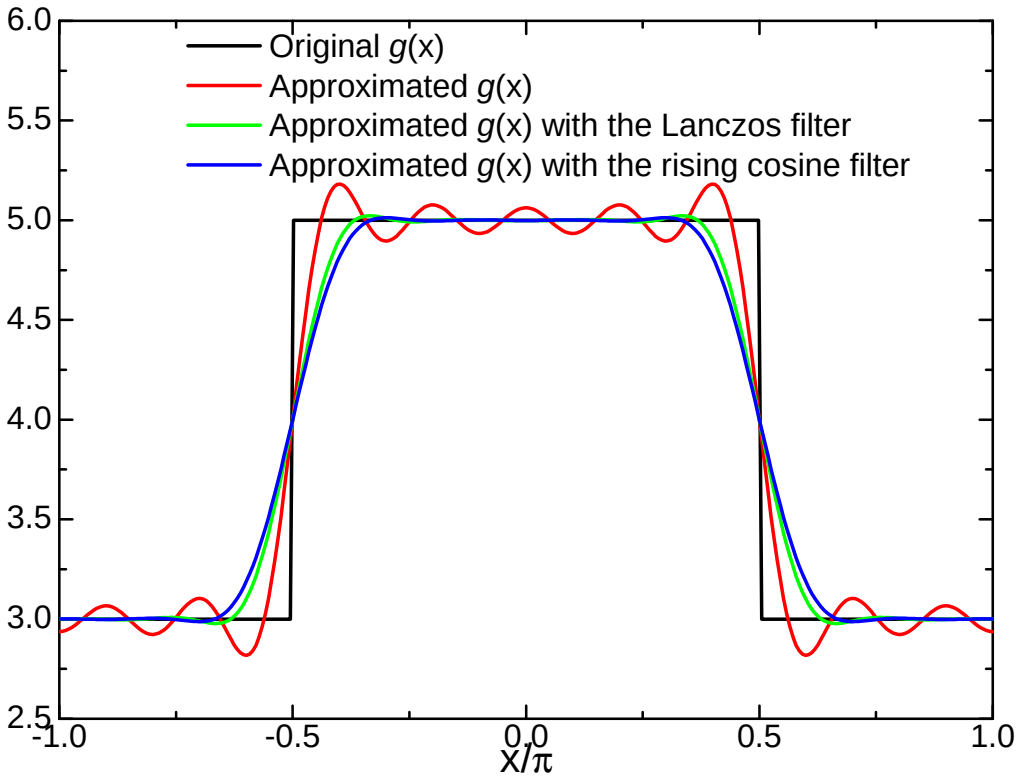

In-plane field components and the effect of the Gibbs phenomenon

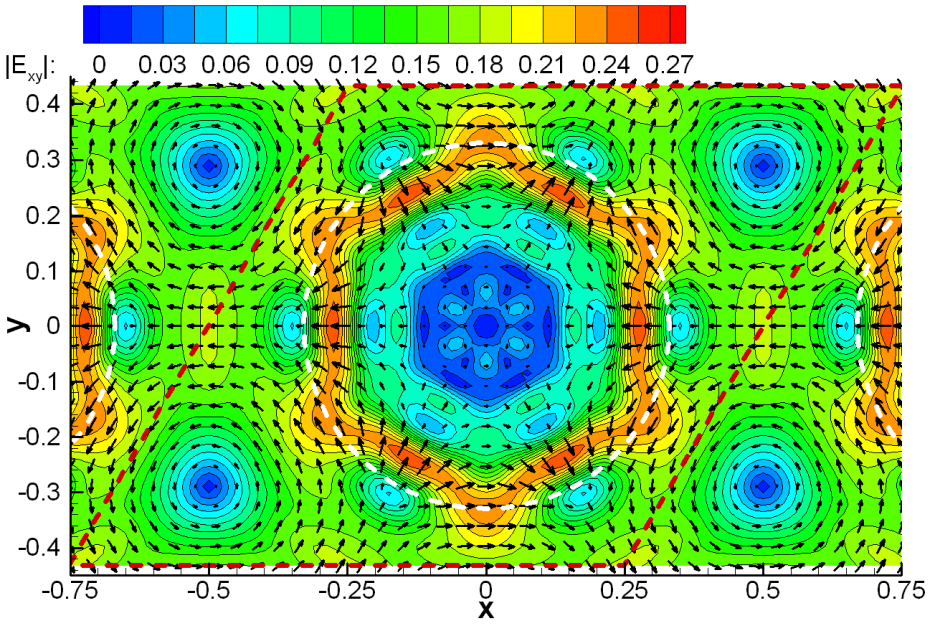

Calculation without the filtering of the permittivity distribution

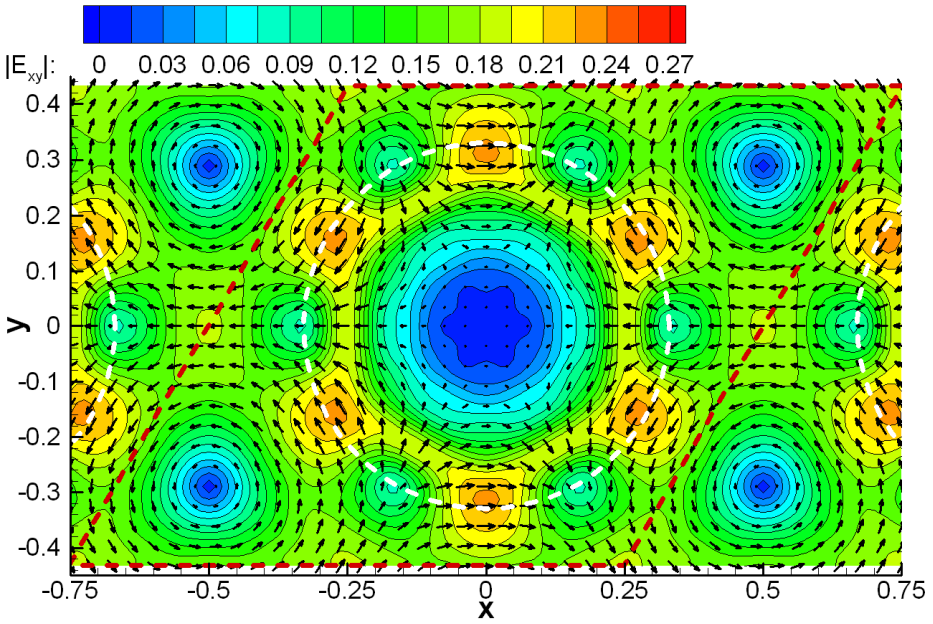

Calculation using the Lanczos filter

Electric field $\mathbf{E}_{xy}$ *amplitude and the direction of the second band TE-polarized Bloch mode with the Bloch vector at the* Γ *point. The photonic crystal consists of the circular air holes (the filling factor f=0.4) in the dielectric slab with the effective refractive index* $n_{eff}=3.24$.

In-plane field components and the effect of the Gibbs phenomenon

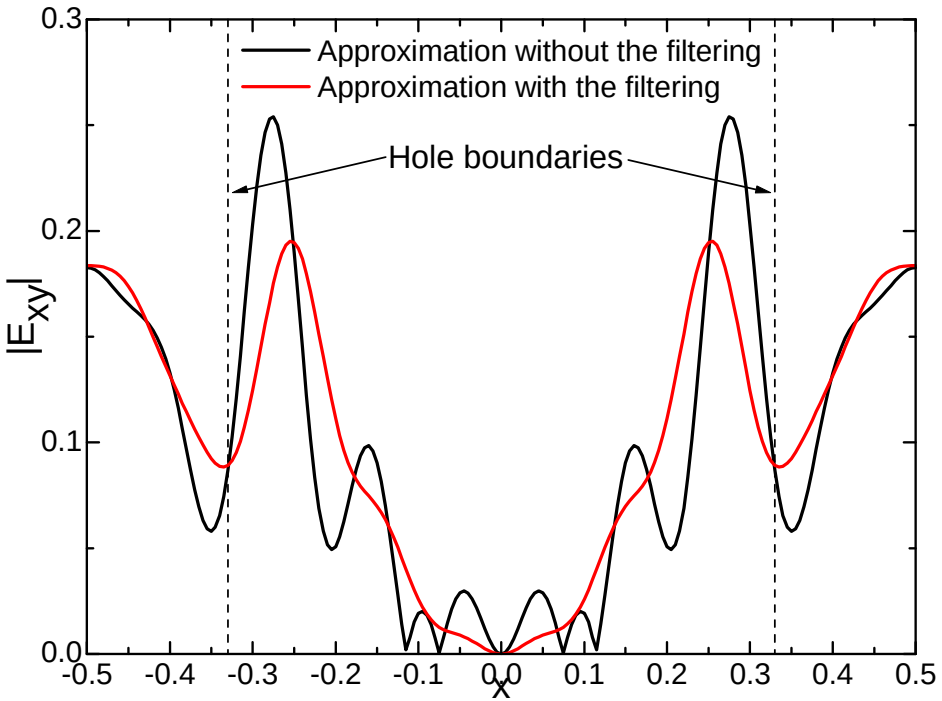

Amplitude of the electric field $\mathbf{E}_{xy}$

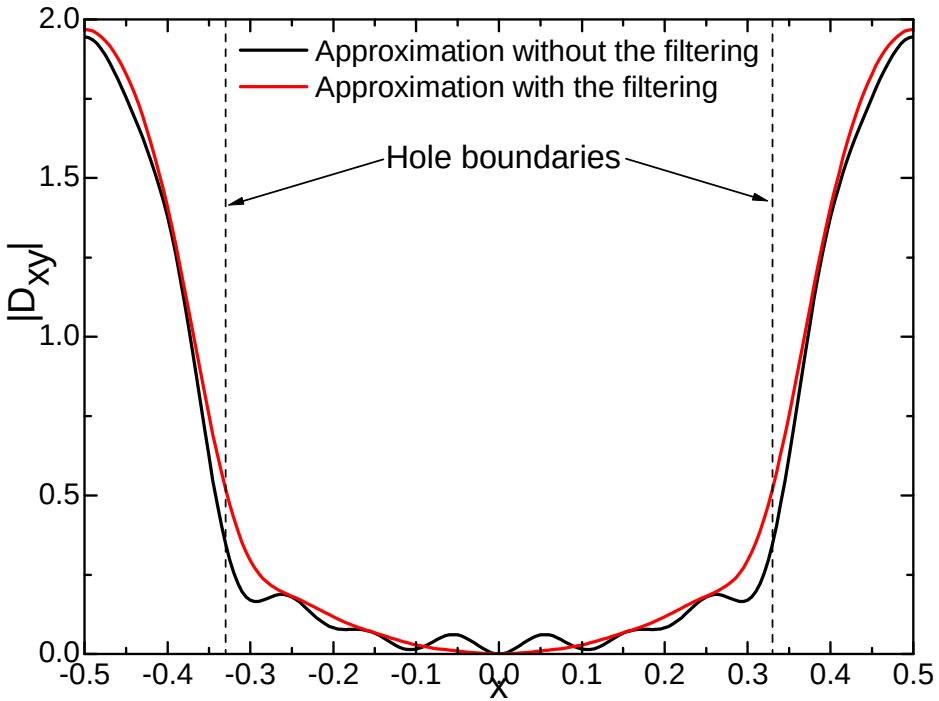

Amplitude of the displacement field $\mathbf{D}_{xy}$

Cross-section along the line y=0 of the electromagnetic field distribution of the second band TE-polarized Bloch mode with the Bloch vector at the Γ point. The photonic crystal consists of the circular air holes (the filling factor f=0.4) in the dielectric slab with the effective refractive index n_{eff}*=3.24.*

Dispersion of the Bloch modes in the PhC

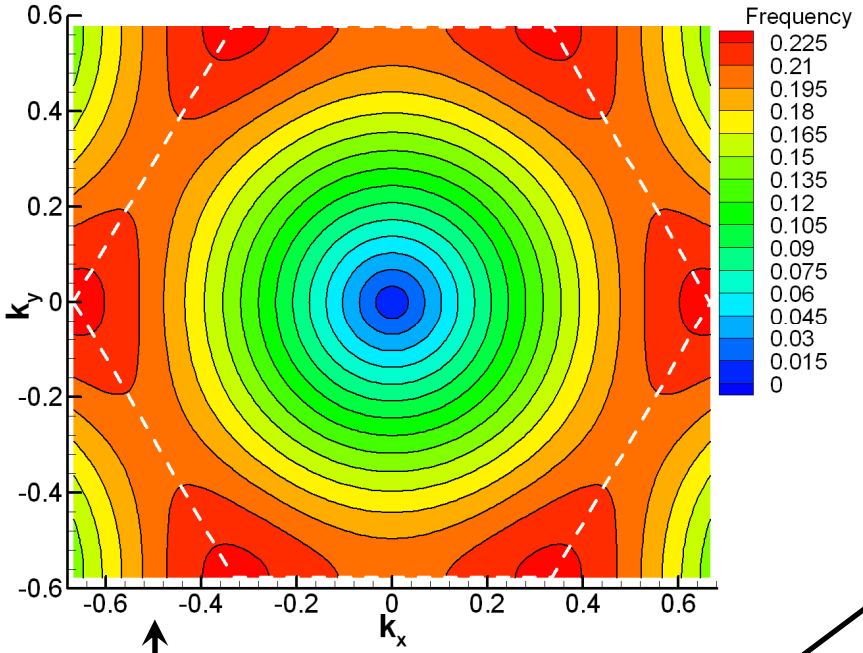

The first band.

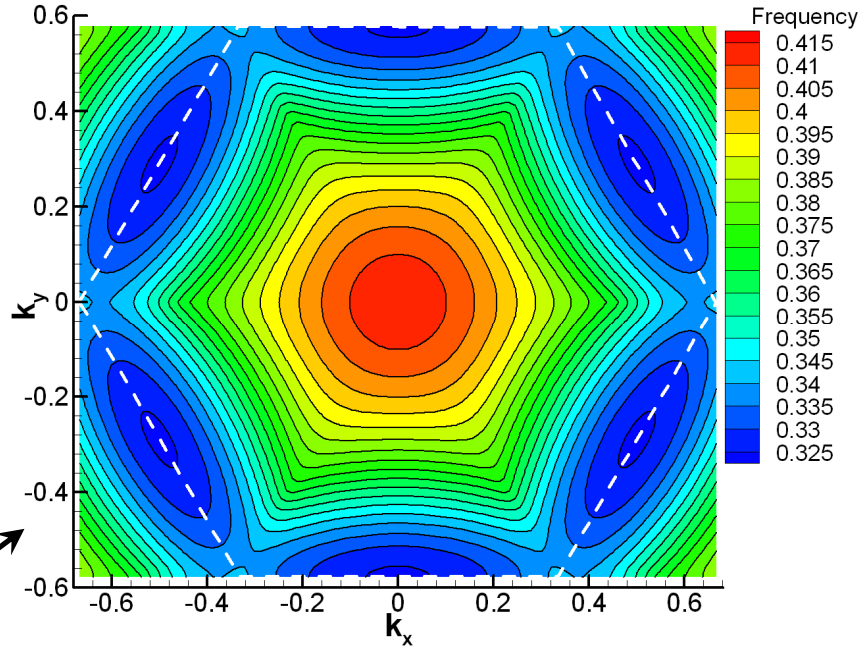

The second band.

The cross-section of the dispersion surfaces

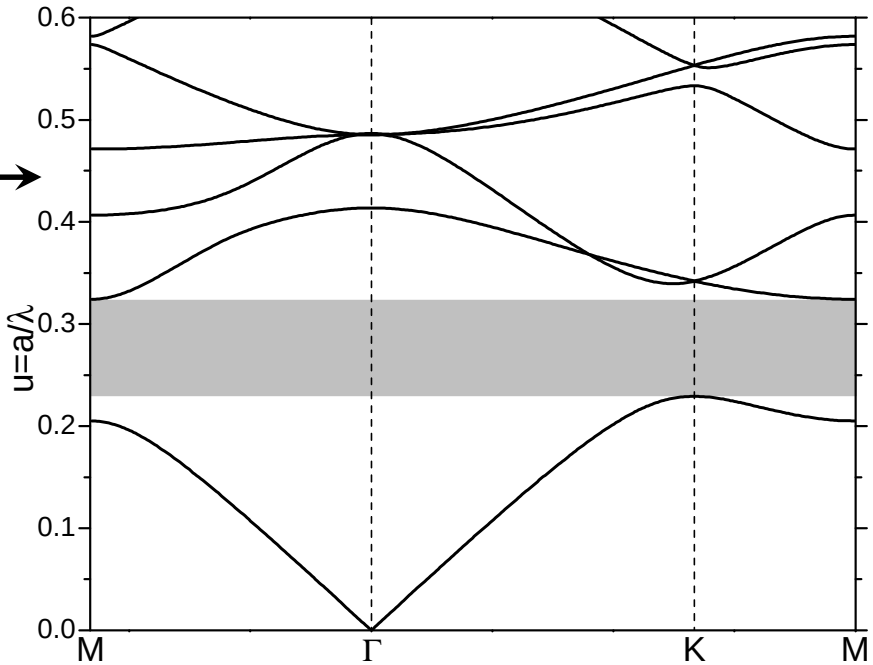

Dispersion of the TE-polarized Bloch modes for the triangular lattice photonic crystal consisting of the circular air holes (the filling factor f=0.4) in the dielectric slab with the effective refractive index n_{eff}=3.24.

Group velocity of the Bloch modes in the PhC

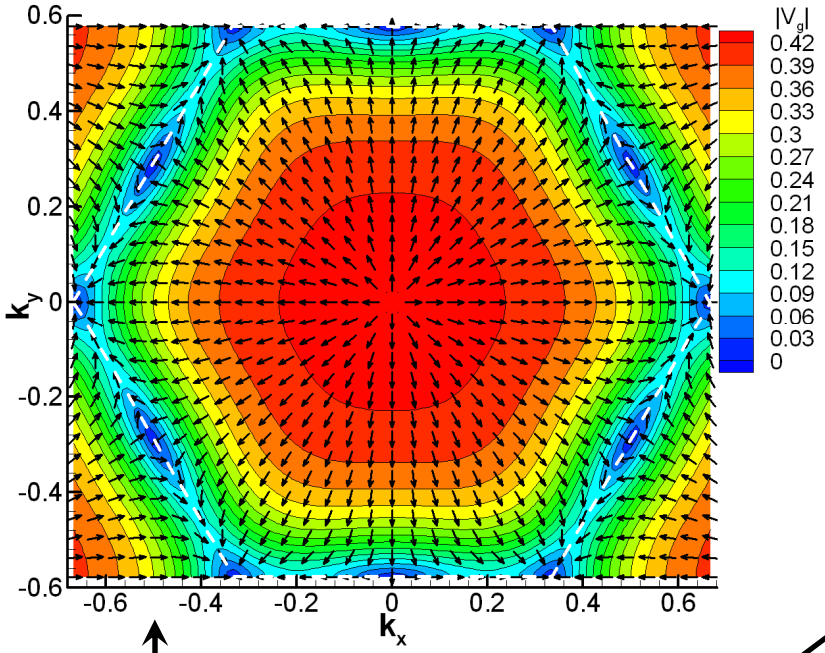

The first band.

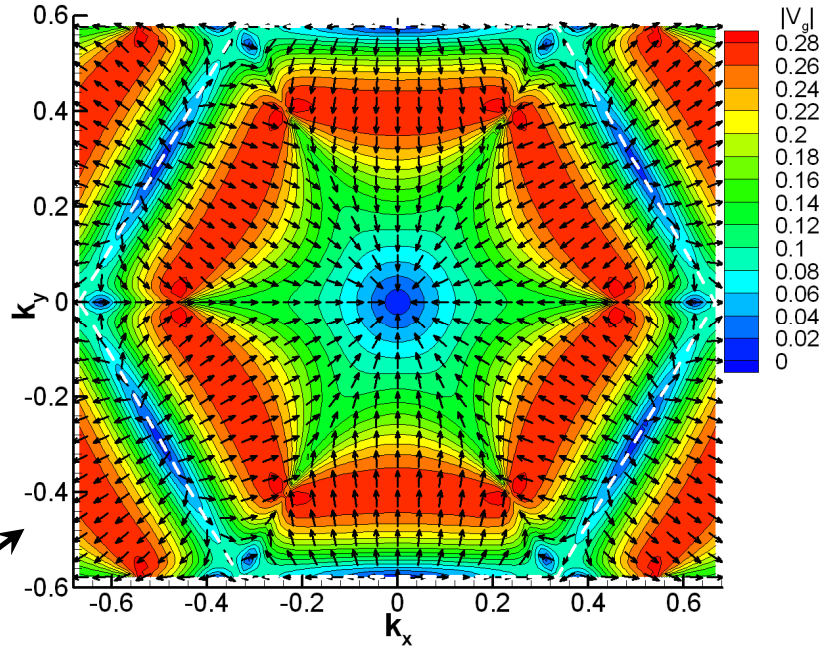

The second band.

The cross-section of the $|\mathbf{V}_g|$ surfaces

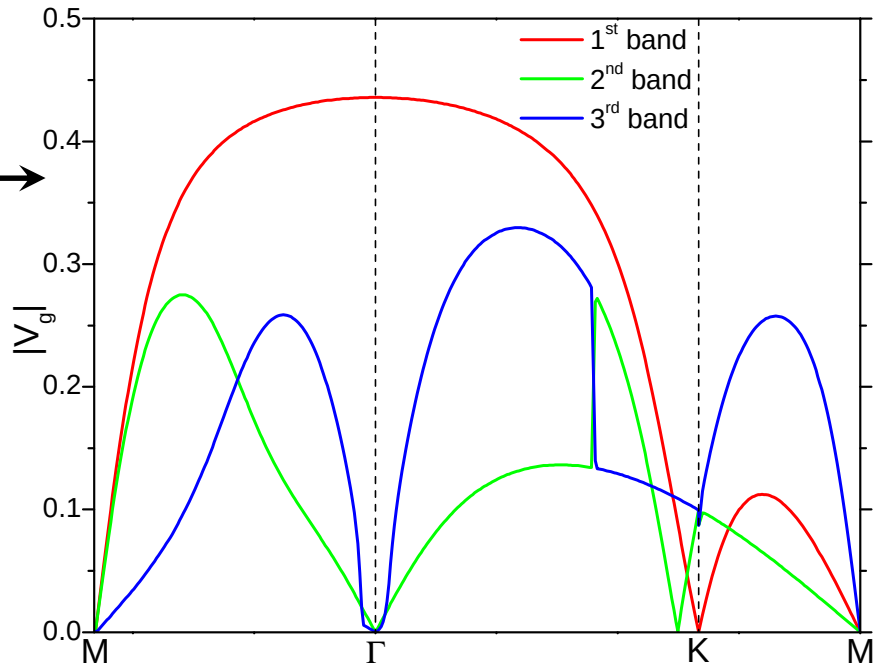

Group velocity of the Bloch modes

$$\mathbf{V}_g = \nabla_{\mathbf{k}} \cdot \omega$$

EFS curvature of the Bloch modes in the PhC

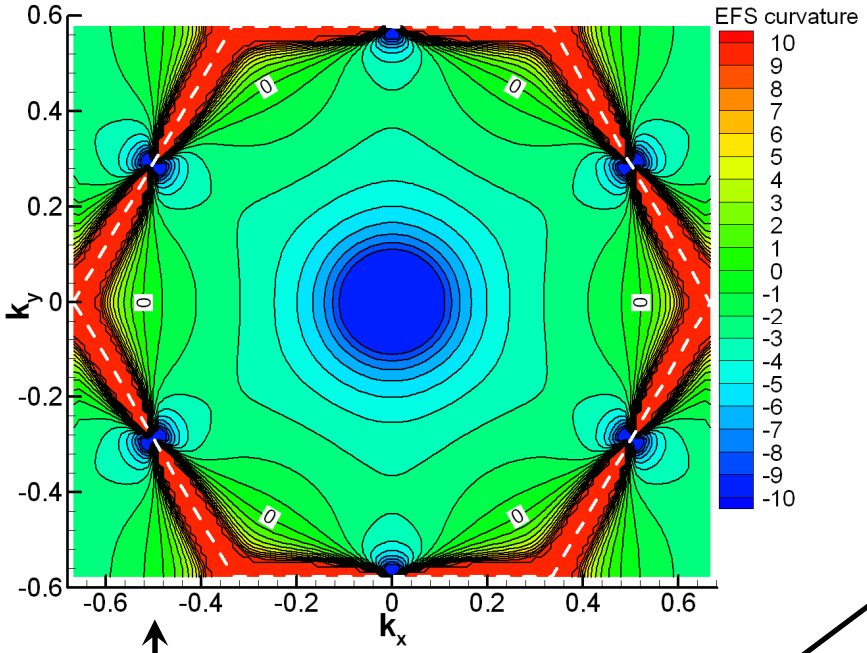

The first band.

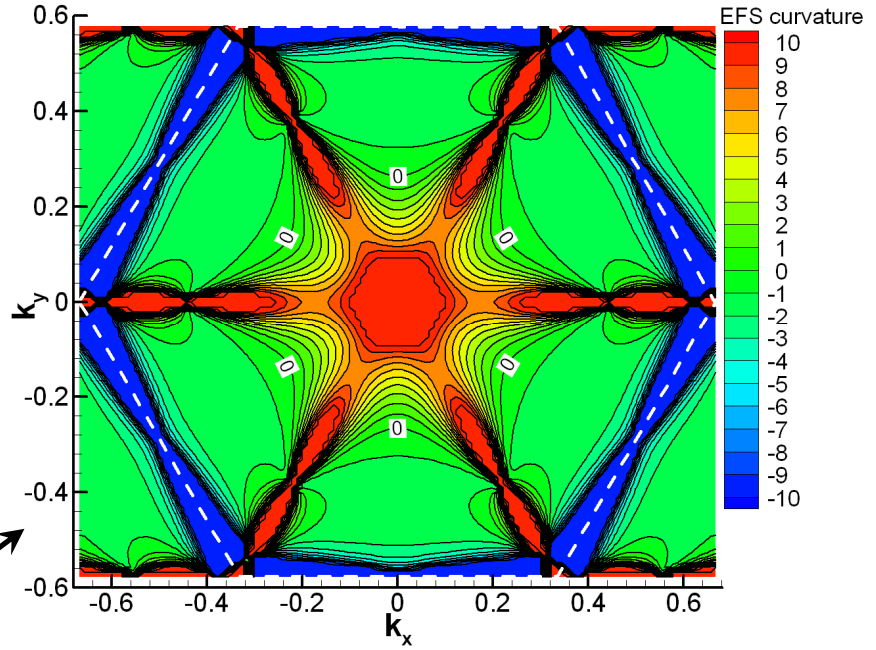

The second band.

The cross-section of the EFS curvature surfaces

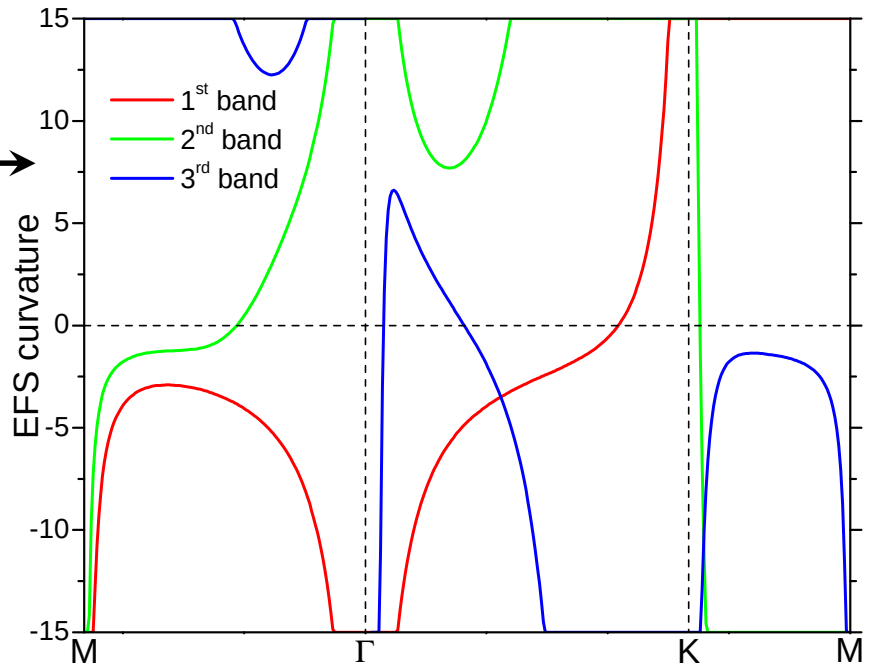

Shape of the EFS determines divergence of the light beams in photonic crystals

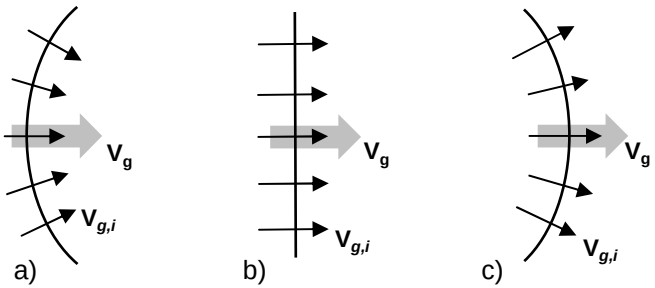

Properties of the guided modes of the planar WG

Field distribution of guided modes propagating in planar waveguides

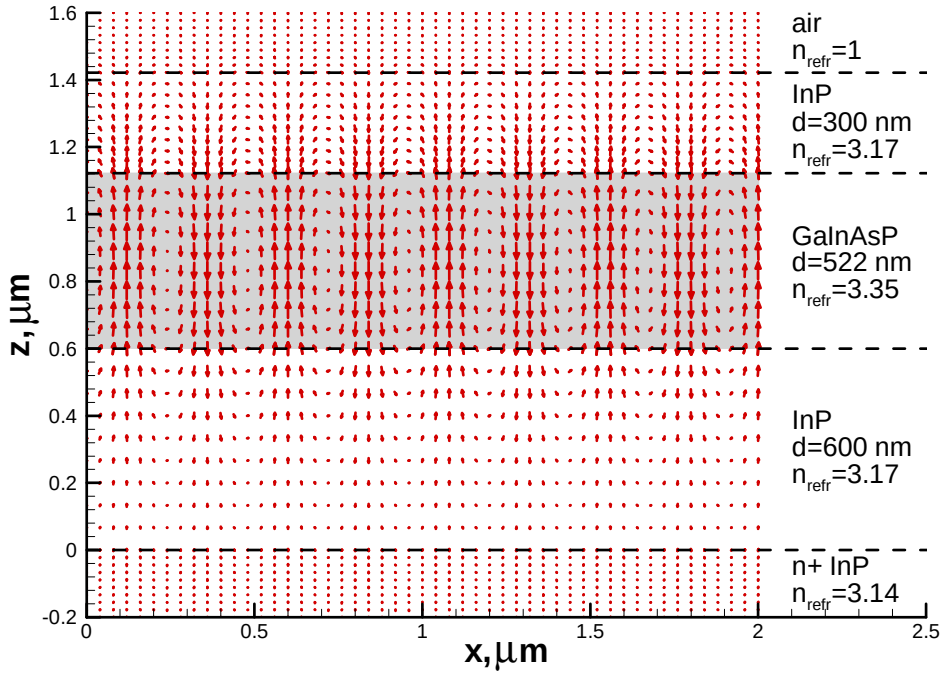

Thick waveguide with low index contrast

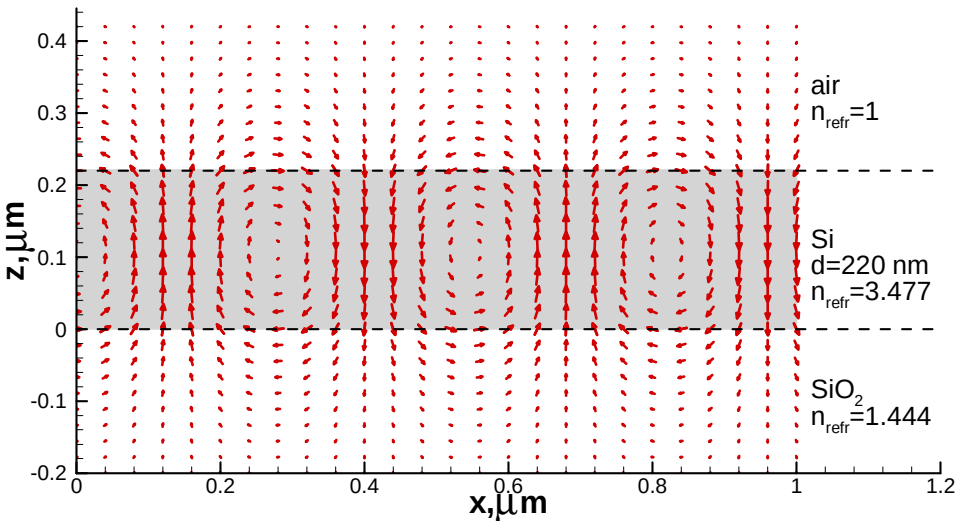

Thin SOI waveguide with high index contrast

Magnetic field distribution $\mathbf{H}_{xz}$ for the *quasi*-TE light polarization.

The Guided Mode Expansion method

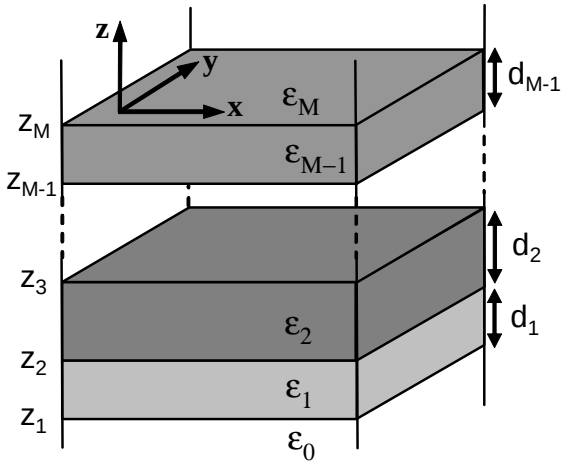

General solution for a guided mode

$$\varphi = \varphi(z)e^{i g x - i \omega t}$$

The magnetic field of a Bloch mode may be expanded using the orthonormal set of the basis states as:

$$\mathbf{H}(\mathbf{r}) = \sum_{\nu} c_\nu \mathbf{H}_\nu(\mathbf{r})$$

The following eigenvalue problem can be derived:

$$\sum_{\nu} \mathbf{W}_{\mu\nu} c_\nu = \frac{\omega^2}{c^2} c_\mu$$

where the elements of the matrix $\mathbf{W}_{\mu\nu}$ *are given by*

$$\mathbf{W}_{\mu\nu} = \int \frac{1}{\varepsilon(\mathbf{r})} \left(\nabla \times \mathbf{H}_\mu^*\right) \cdot \left(\nabla \times \mathbf{H}_\nu\right) d\mathbf{r}$$

Comparison of the Guided Mode Expansion and the Plane Wave Expansion methods

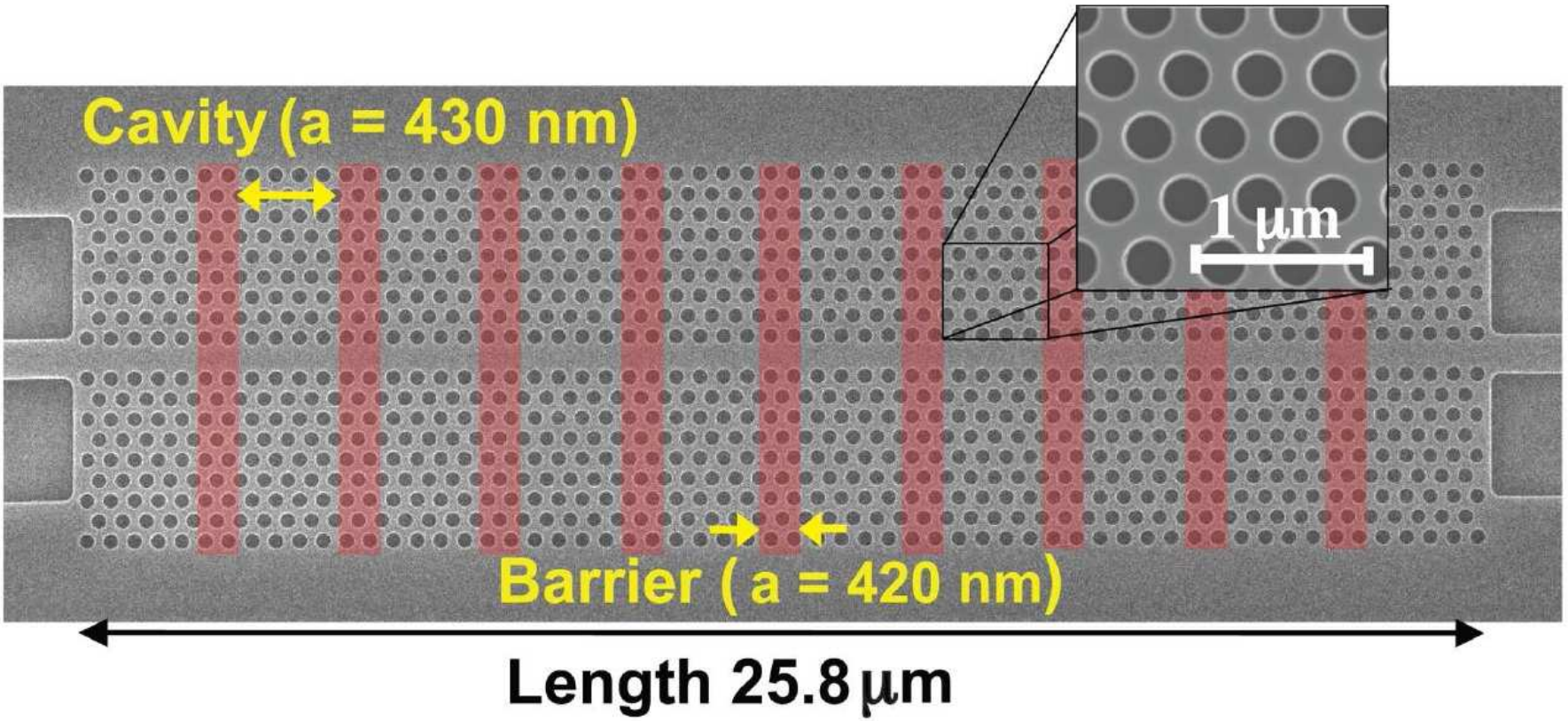

Top-view scanning electron microscope (SEM) image of the heterostructure coupled-cavity waveguide (CCW) fabricated using an SOI structure. The hole filling factor in the cavity f=40%.

Comparison of the Guided Mode Expansion and the Plane Wave Expansion methods

Experimental dispersion diagram of the CCW waveguide compared with the Plane Wave Expansion and the Guided Mode Expansion calculations.

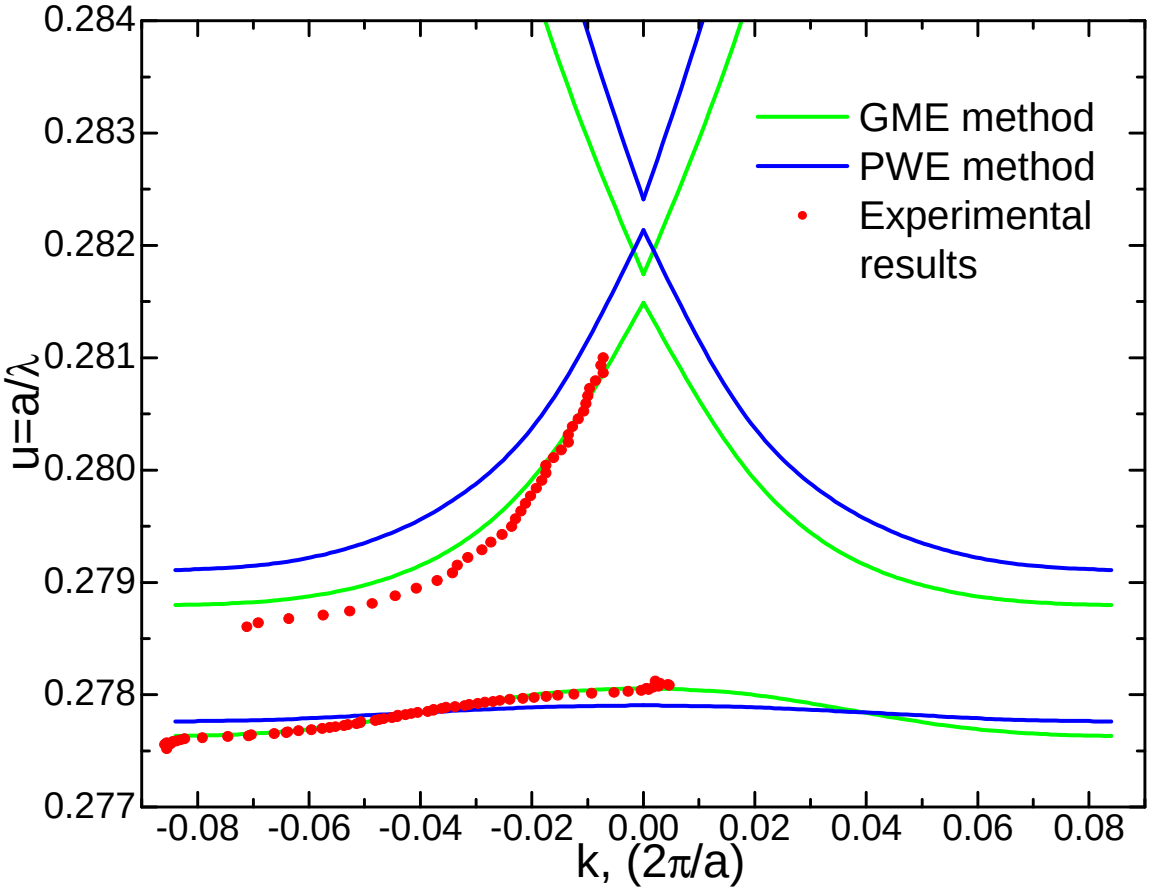

The effective refractive index of the SOI waveguide n_{eff}=2.8278 (for λ=1.55 μm) have been used for the PWE calculation.

J. Jágerská et al., Opt. Lett. v.34 n.3 (2008)

The effect of the small variation of the permittivity distribution on the PhC optical properties

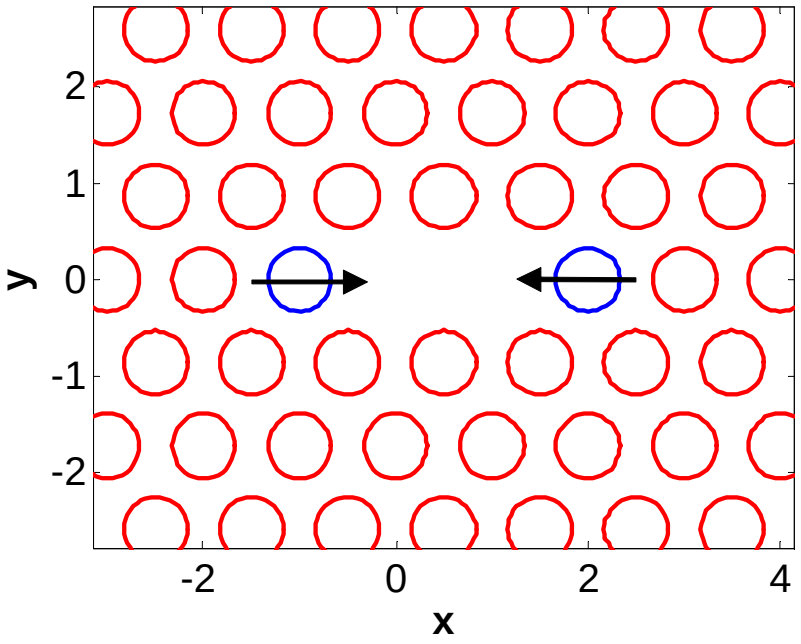

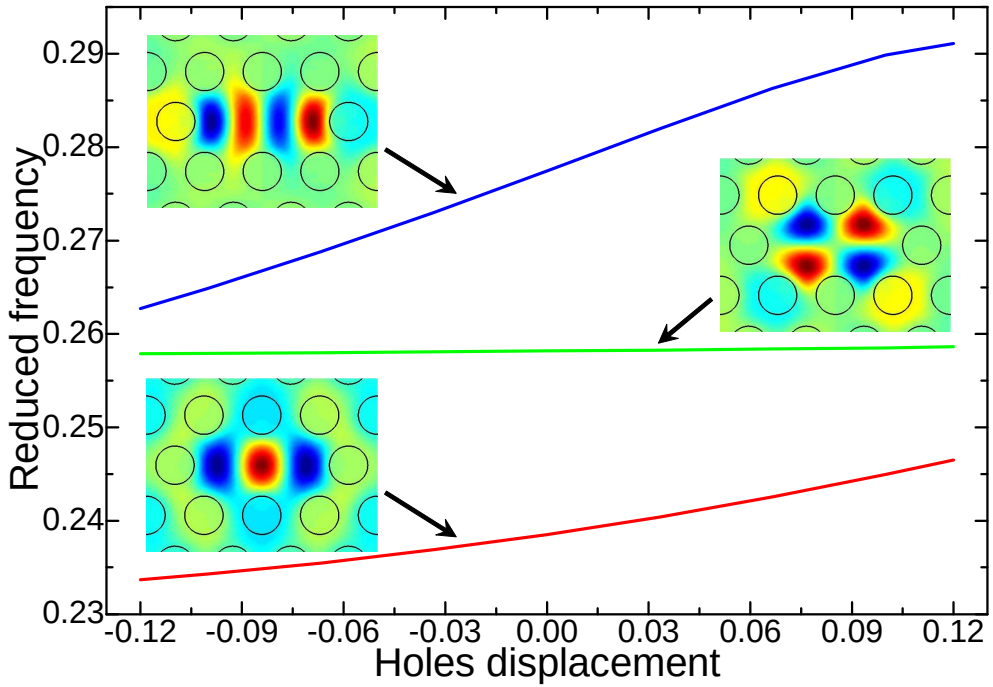

Modelling of the effect of the cavity shape change on the localized states properties usually requires series of calculations for each geometry.

Utilization of the perturbation theory can significantly reduce amount of calculations required for the structure design and optimization.

The perturbation of the permittivity distribution

Variation of the material permittivity

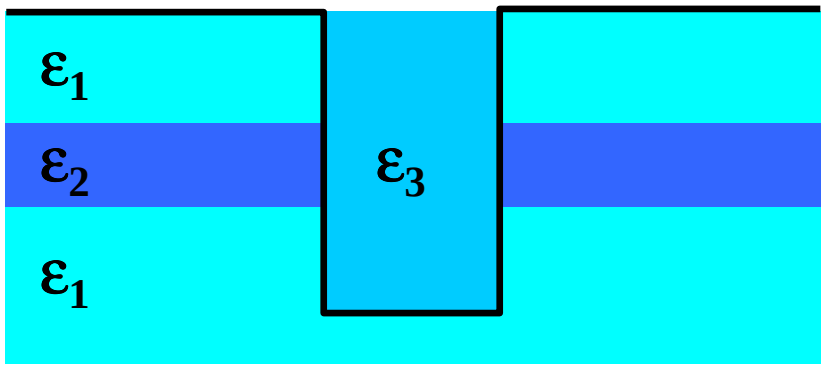

$$\varepsilon_3 \rightarrow \varepsilon'_3$$

Variation of the hole/pillar size

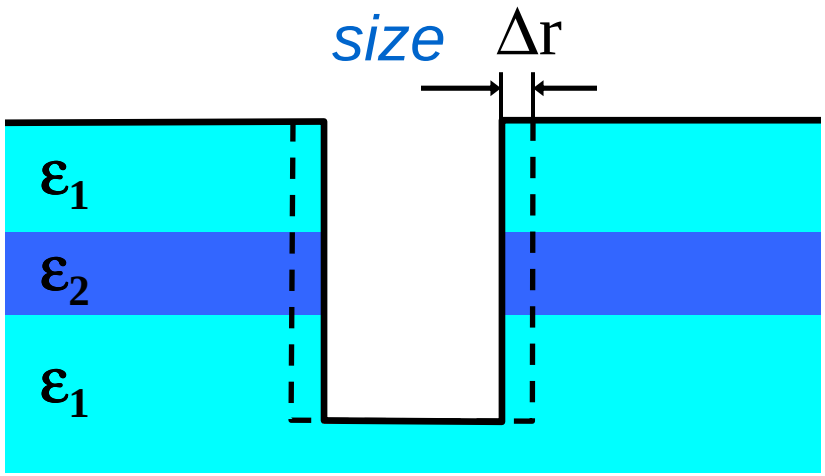

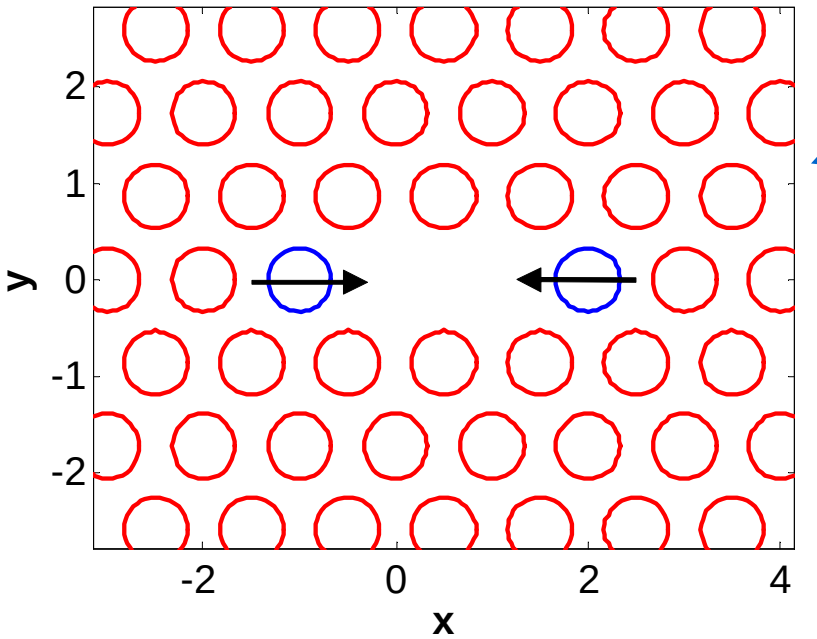

Variation of the hole/pillar position

Even a small change of photonic crystal parameters can lead to a discontinues perturbation of the permittivity distribution.

The perturbation of the permittivity distribution

Shifting boundaries

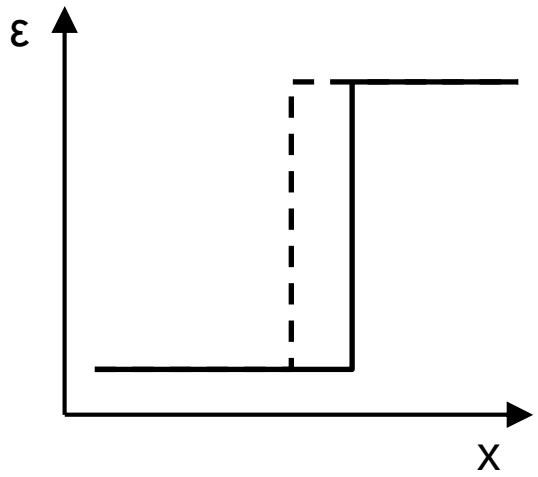

Discontinuous change of the permittivity

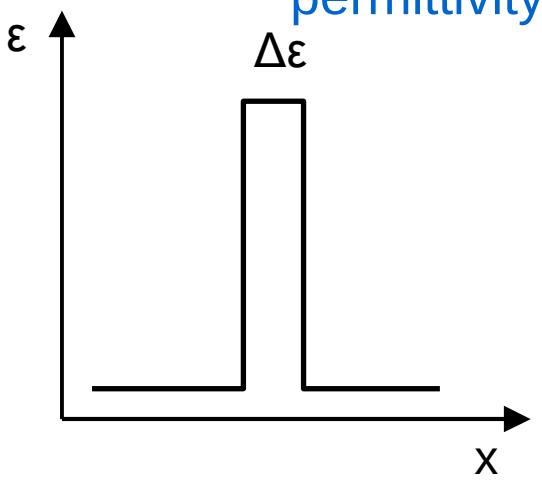

The series of the correction terms don't converge even for a small shift of the boundary with high index contrast

The coefficients of the decomposition of the permittivity can be defined as functions of variables in the multidimensional parametric space

$$\varepsilon(\mathbf{k}) = \varepsilon(\mathbf{k}, \mathbf{x})$$

Analytical expressions for the derivatives $\nabla_{\mathbf{x}} \cdot \varepsilon$ *and* $(\nabla_{\mathbf{x}})^2 \cdot \varepsilon$ *allow us to introduce continuous variations of the permittivity and ensure convergence of the perturbation series*

Calculation the effect of the permittivity distribution variations

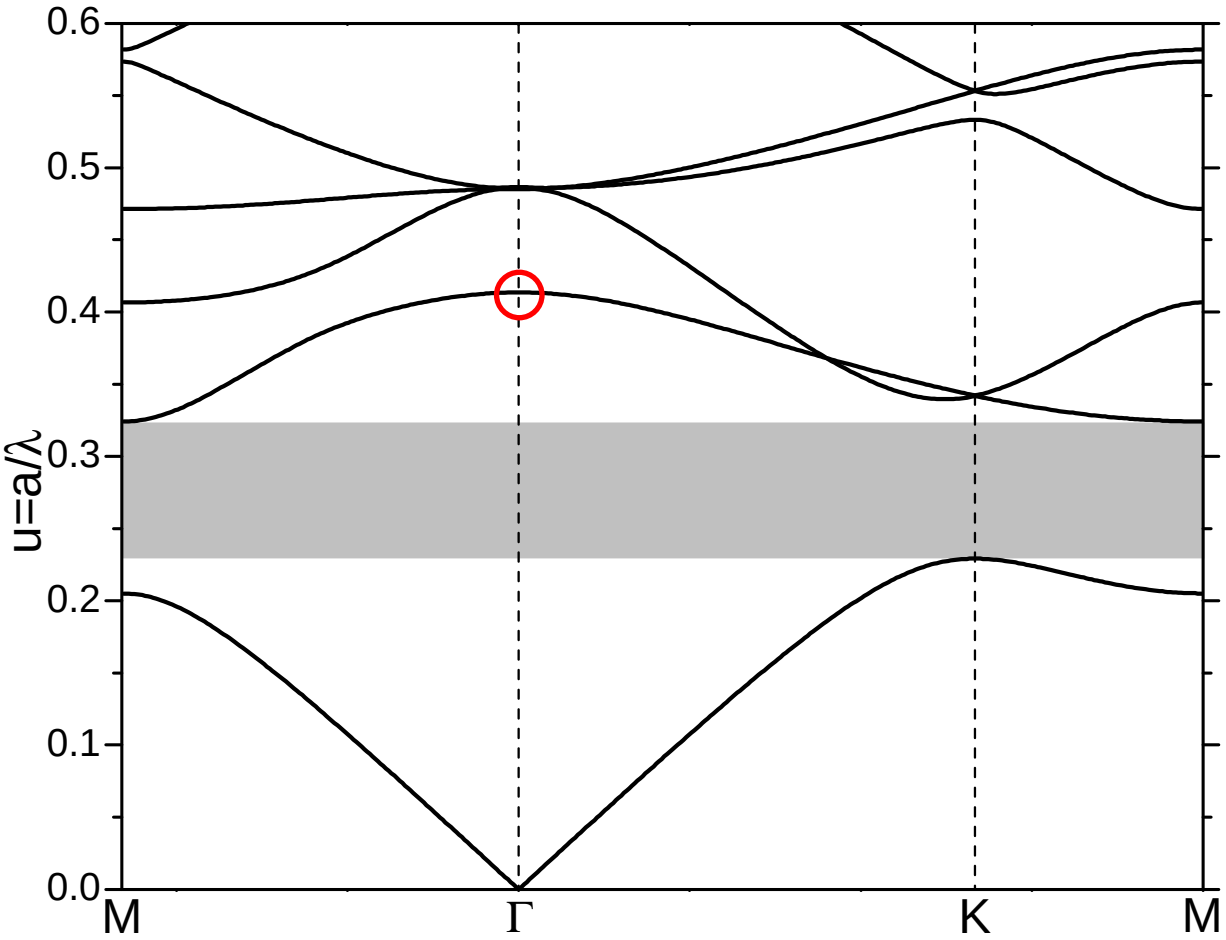

Dispersion of the TE-polarized Bloch modes for the triangular lattice photonic crystal consisting of the circular air holes (the filling factor f=0.4) in the dielectric slab with the effective refractive index n_{eff}=3.24.

The effect of the order of the perturbation method

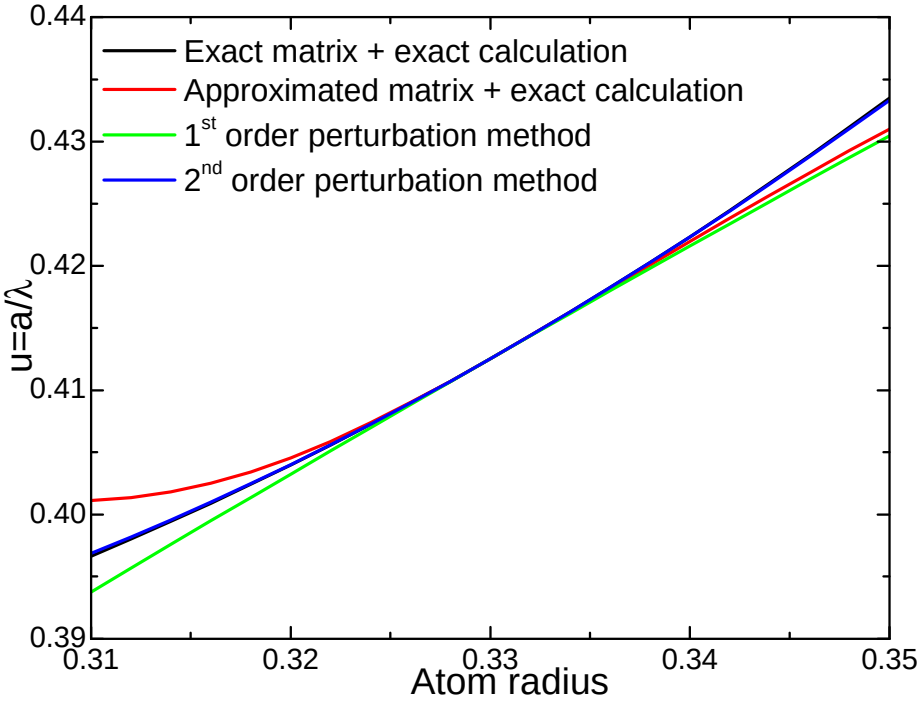

Dependence of the Bloch mode frequency on the variation of the hole size for different orders of the perturbation method.

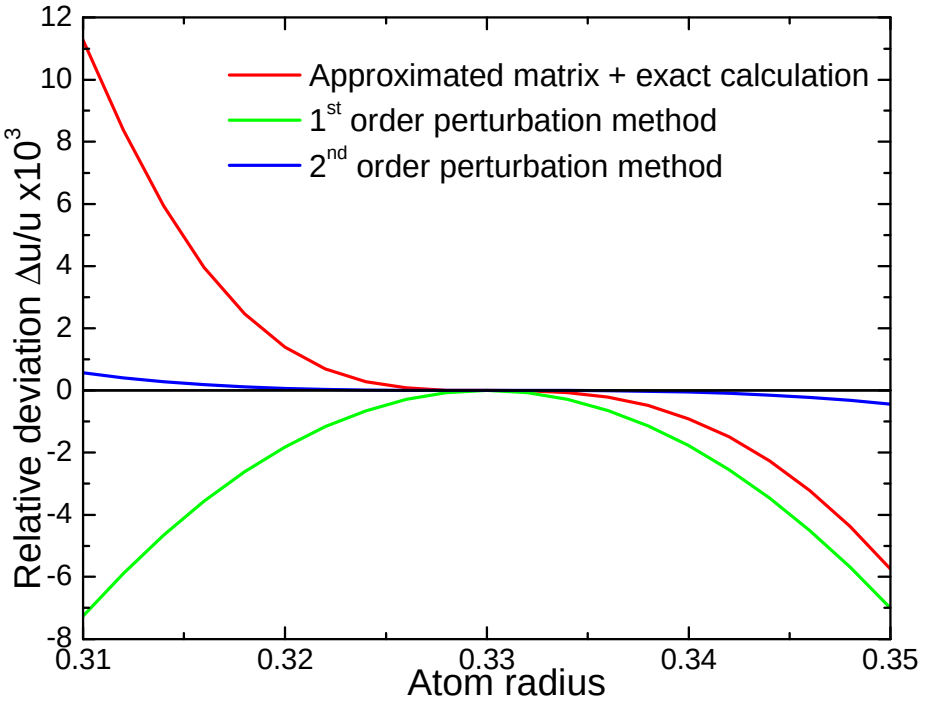

Relative error of the mode frequencies calculated with the perturbation method.

Tuning the dispersion of the W1 waveguide

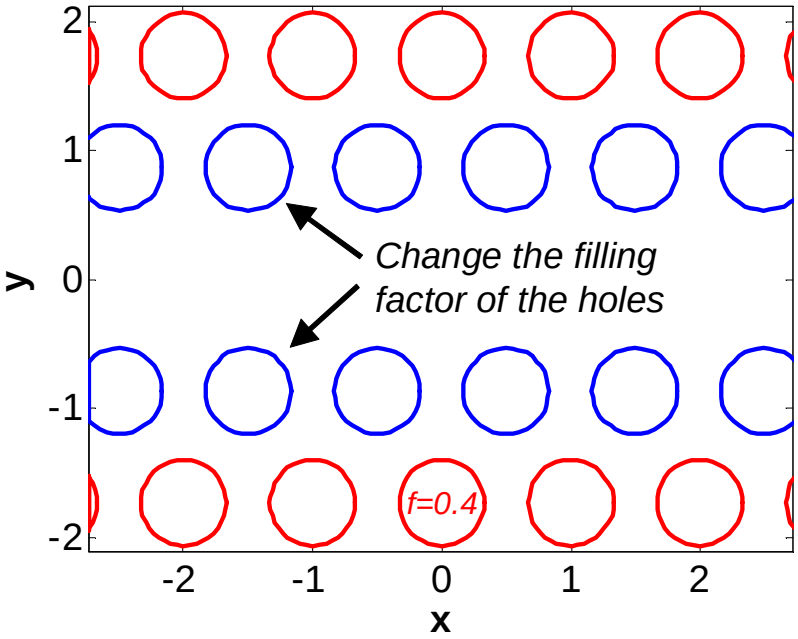

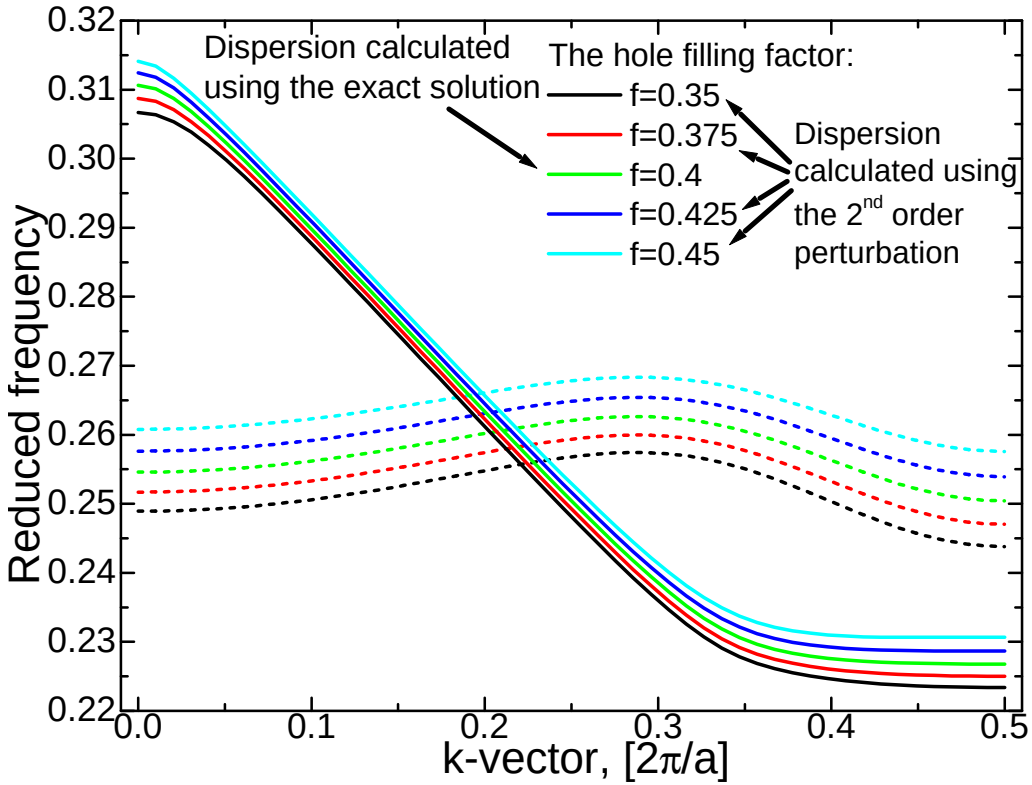

Tuning the dispersion of the W1 waveguide

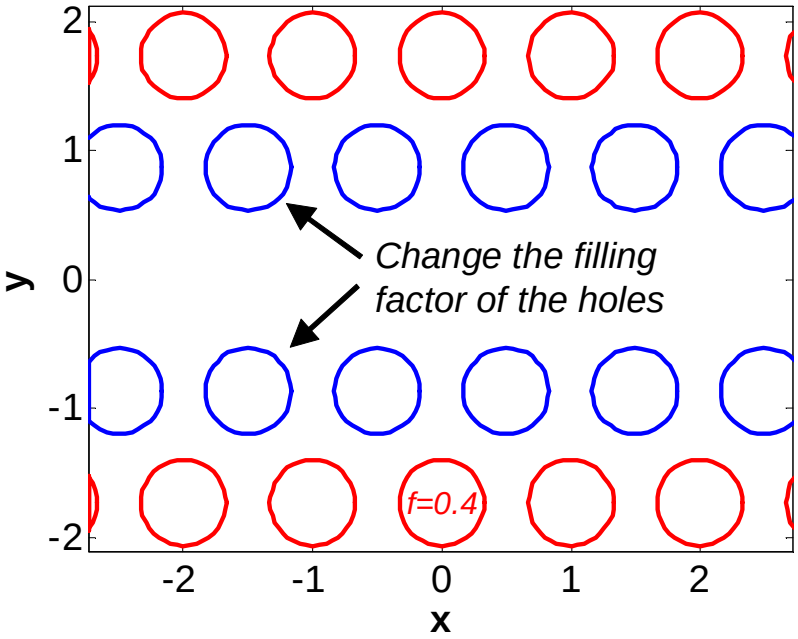

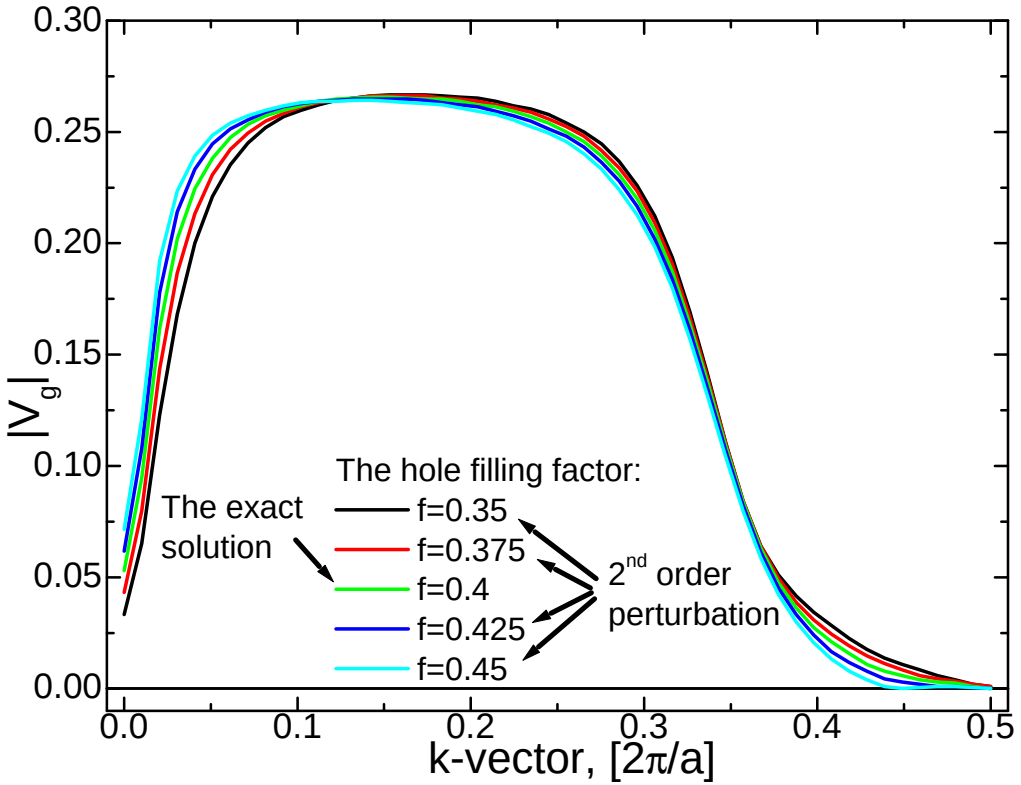

Utilization of the perturbation theory allows us to estimate the effect of the variations of the photonic crystal parameters on the structure optical properties. High computational speed and good accuracy help to speed-up design and optimization of photonic crystal based structures.

Summary

- *The Bloch vector based and the frequency based Plane Wave Expansion methods have been derived and used for analysis of the propagating and evanescent modes in photonic crystals.*
- *The effect of the discontinuity of the distribution of the dielectric permittivity and/or the magnetic permeability in the photonic crystal have been discussed and new methods to improve the accuracy have been proposed.*
- *The Guided Mode Expansion method, which take into account vertical light confinement in 2D photonic crystals, has been developed and used for analysis of SOI and membrane based photonic crystals.*
- *A new method of analysis of small variations of photonic crystal parameters has been developed. This approach is based on the combination of the mode expansion method and the perturbation theory.*

Analysis of silicon single crystal quality

- *Introduction. Crystal growth from the melt. Czochralski method.*
- *Thermo-elastic stress in growing crystals.*
- *Initial defect incorporation into silicon crystals.*
- *Point defect nucleation and evolution during crystal growth.*

Silicon single crystals grown by Czochralski method

Schematic model of Czochralski method

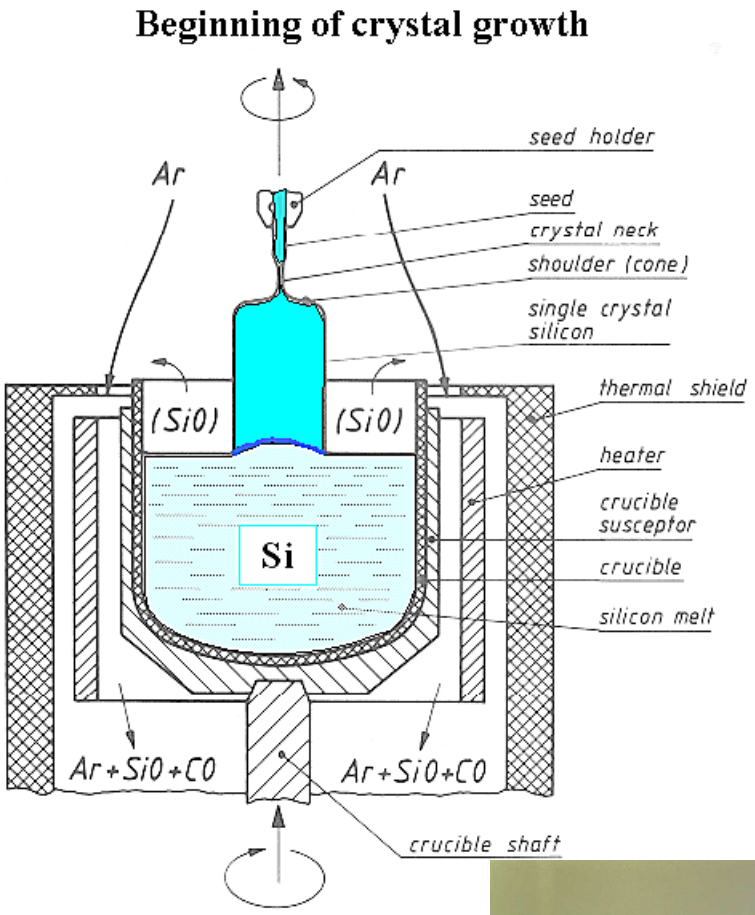

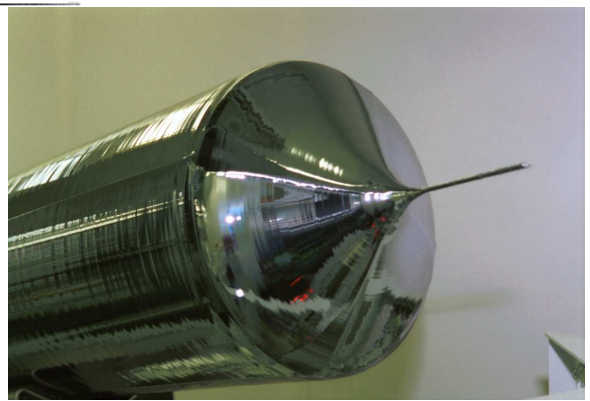

300 mm silicon single crystals grown by Wacker Siltronics AG, weight 250 kg

WACKER

Stress tensor for the 3D case

Displacement tensor

$$u_{ik} = \frac{1}{2}\left(\frac{\partial u_i}{\partial u_k} + \frac{\partial u_k}{\partial u_i}\right)$$

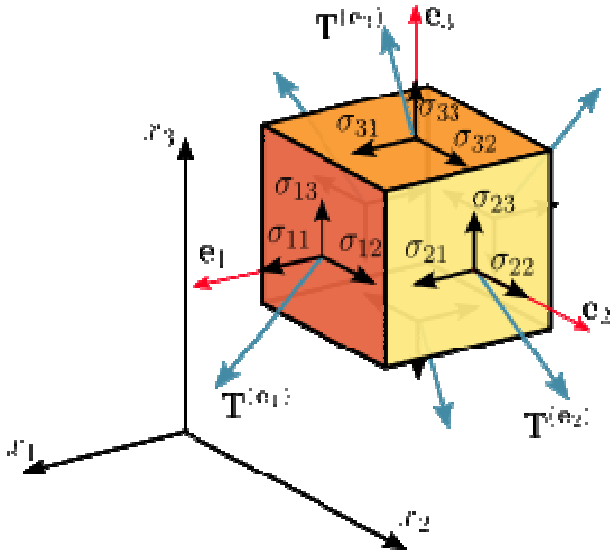

Stress tensor and the Hooke's law

$$\sigma_{ik} = C_{iklm} u_{lm}$$

Thermal expansion correction

$$\sigma_{ik} = C_{iklm}(u_{lm} - u^T_{lm})$$

Equilibrium condition

$$\frac{\partial \sigma_{ik}}{\partial x_k} + W_i = 0$$

The principal stress components

$$\left|\sigma_{ij} - \lambda\delta_{ij}\right| = \begin{vmatrix} \sigma_{11}-\lambda & \sigma_{12} & \sigma_{13} \\ \sigma_{21} & \sigma_{22}-\lambda & \sigma_{23} \\ \sigma_{31} & \sigma_{32} & \sigma_{33}-\lambda \end{vmatrix} = 0$$

$$\sigma_{ij} = \begin{bmatrix} \sigma_1 & 0 & 0 \\ 0 & \sigma_2 & 0 \\ 0 & 0 & \sigma_3 \end{bmatrix}$$

Von Mises stress

Von Mises stress

$$\tau = \sqrt{\frac{1}{2}\left((\sigma_1 - \sigma_2)^2 + (\sigma_1 - \sigma_3)^2 + (\sigma_2 - \sigma_3)^2\right)}$$

The yield criterion

$$f(\tau) = \tau - k = 0$$

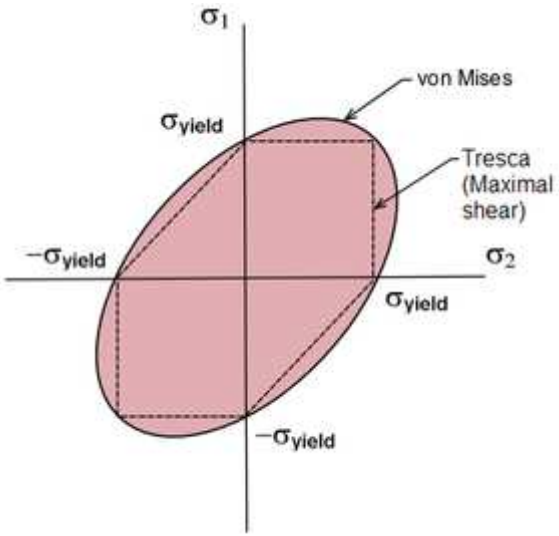

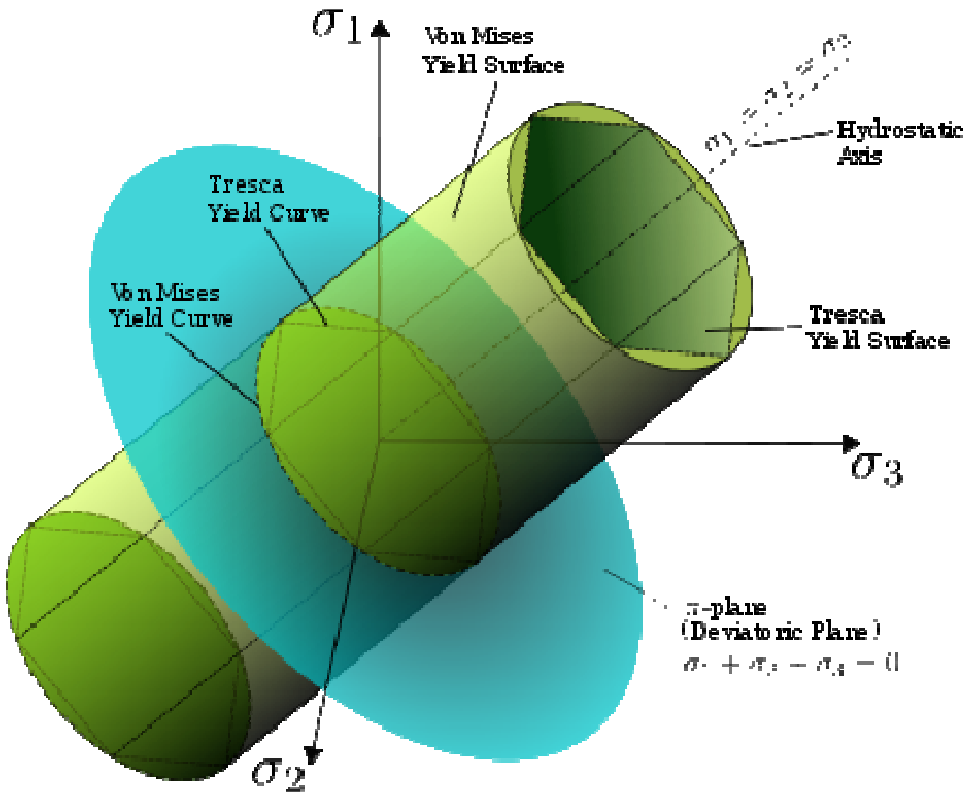

Von Mises stress in silicon single crystals

Temperature distribution

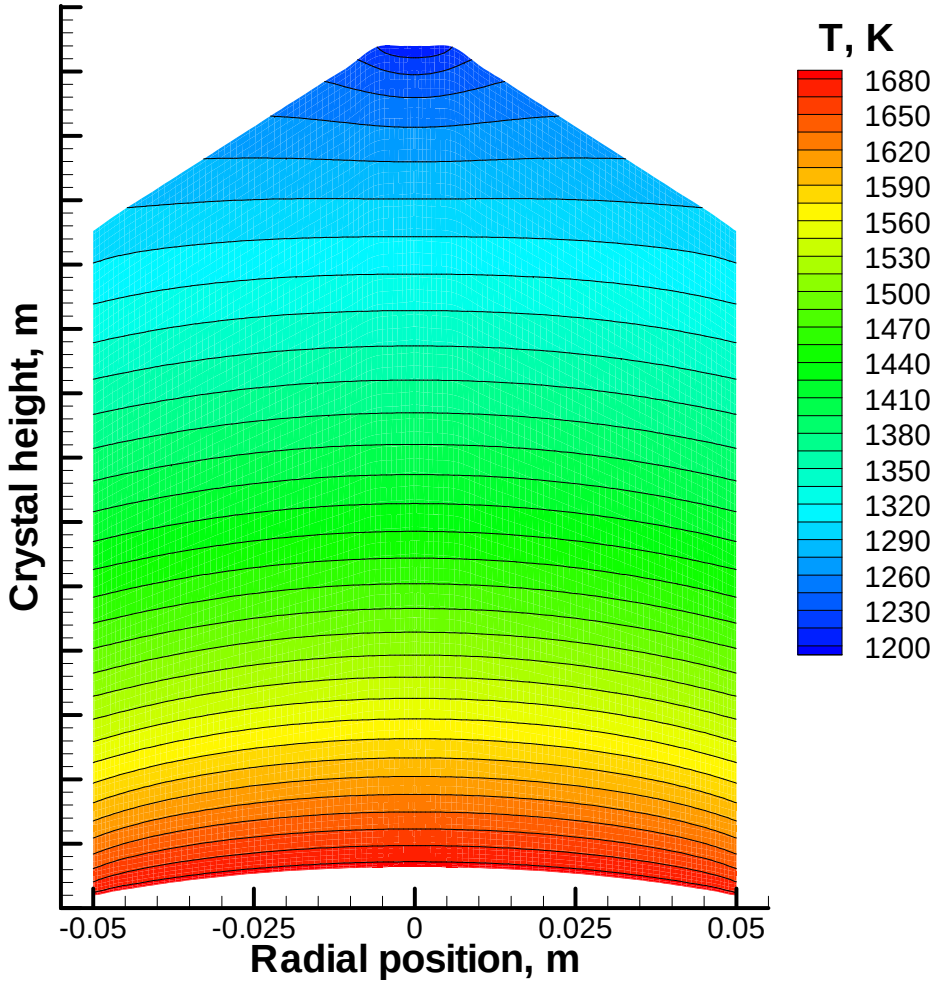

Temperature gradient distribution

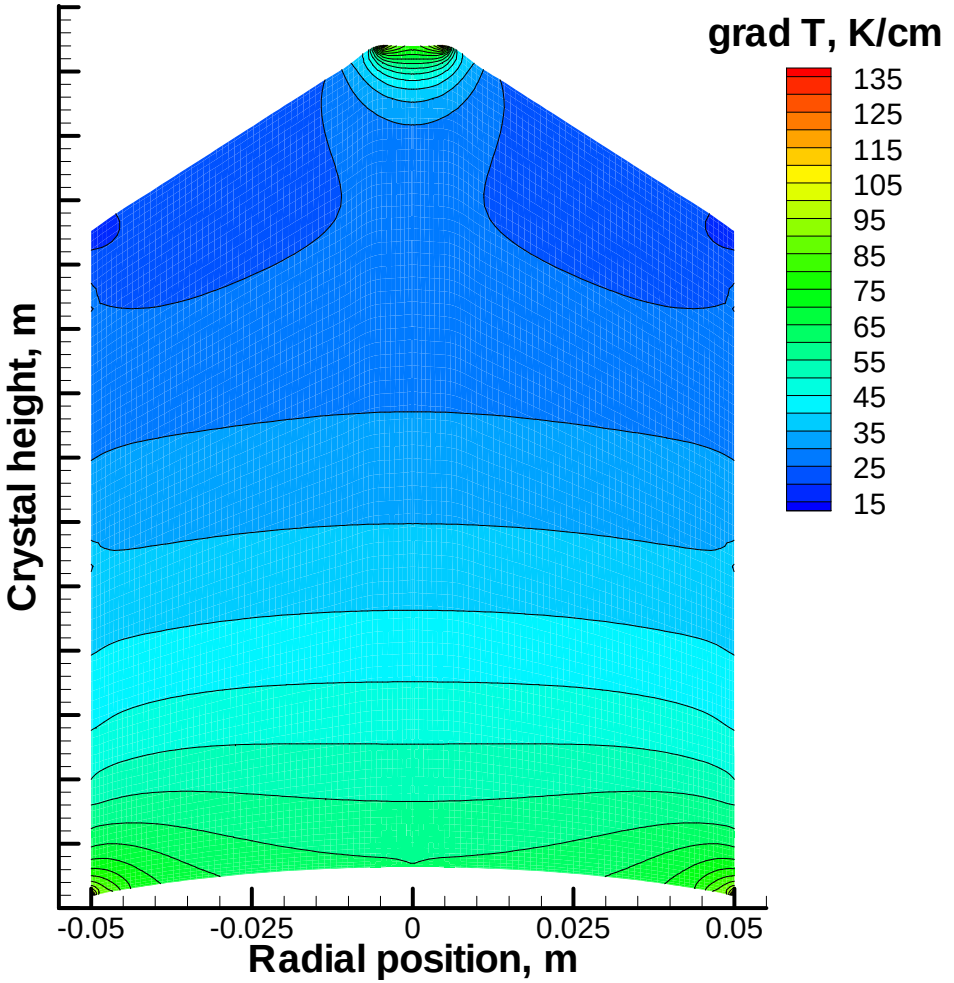

A silicon single crystal grown by Czochralski method

Von Mises stress in silicon single crystals

Crystal height 132 mm

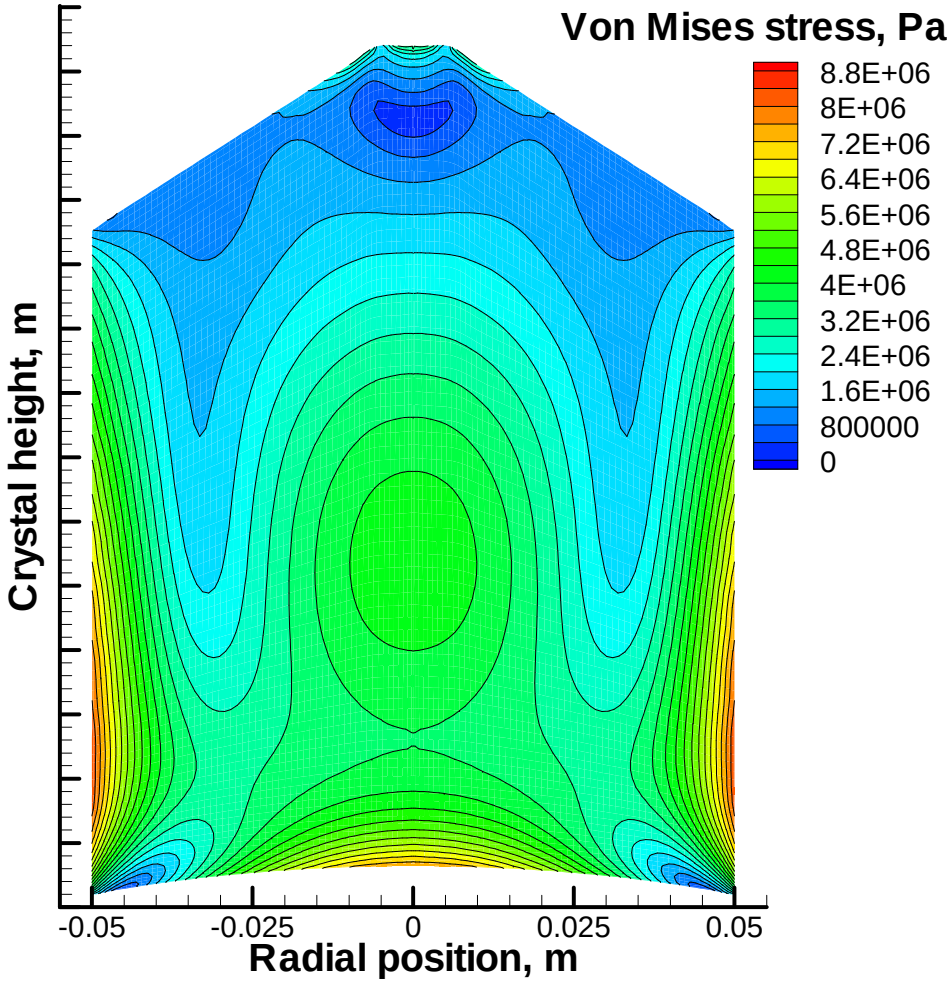

Crystal height 332 mm

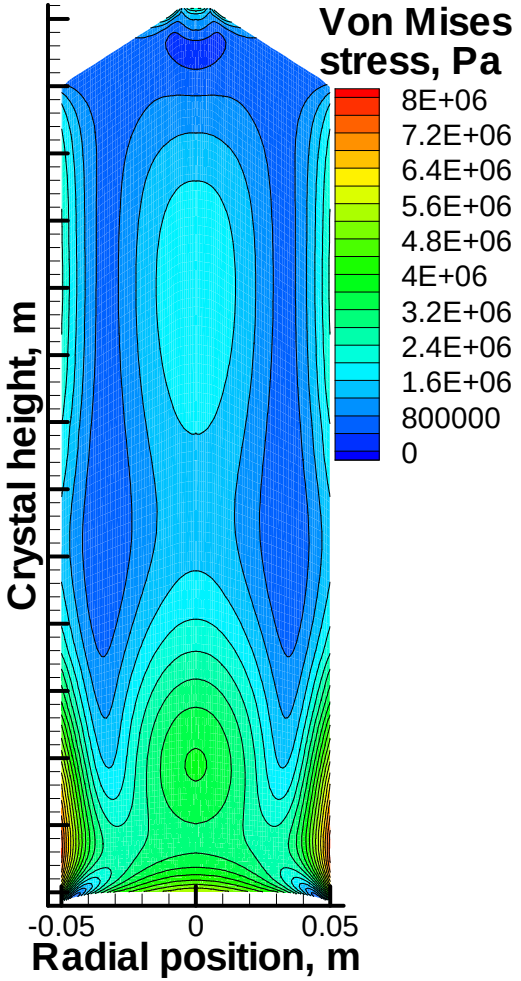

Silicon single crystals grown by Czochralski method

Point defects in silicon single crystals

Si wafer after etching + copper decoration

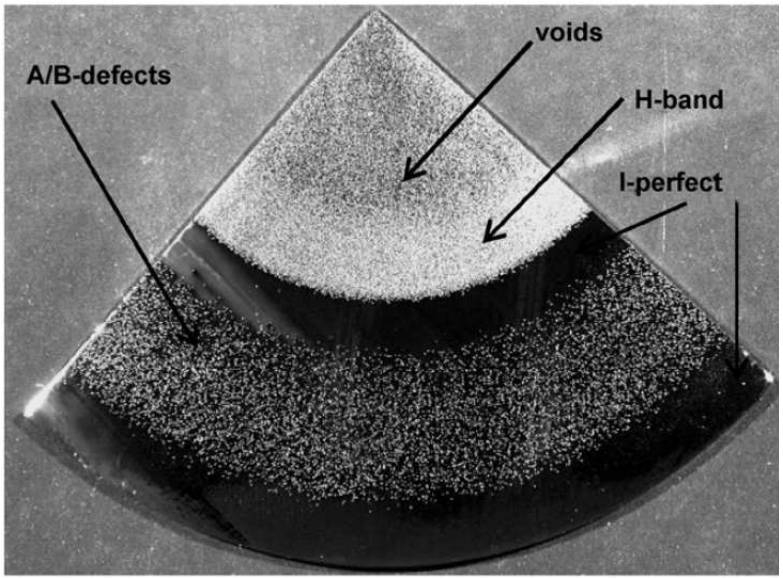

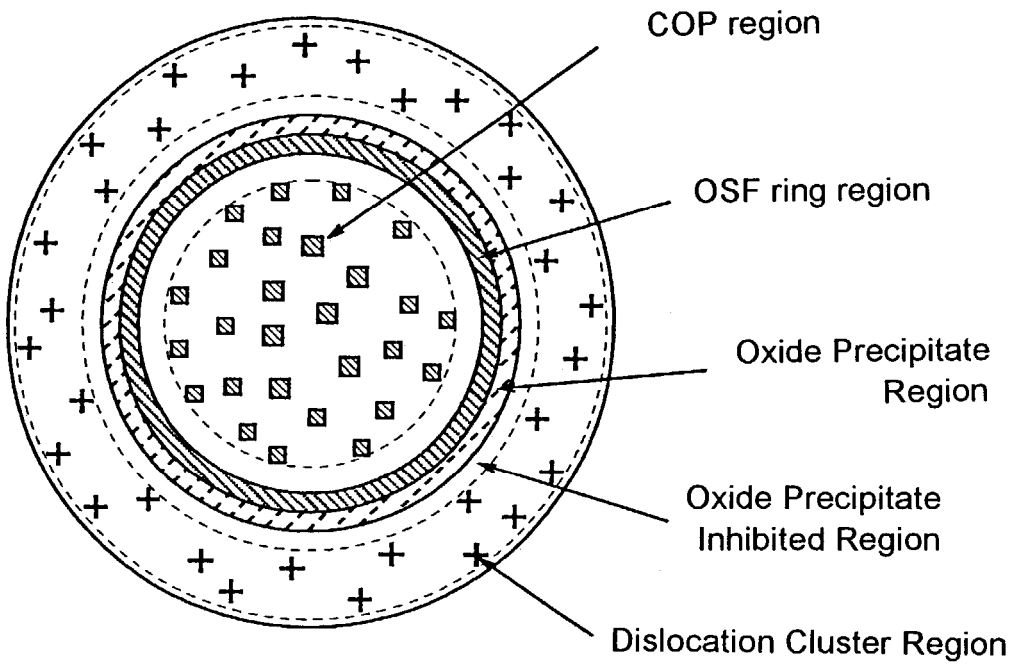

Schematic view of point defects formation

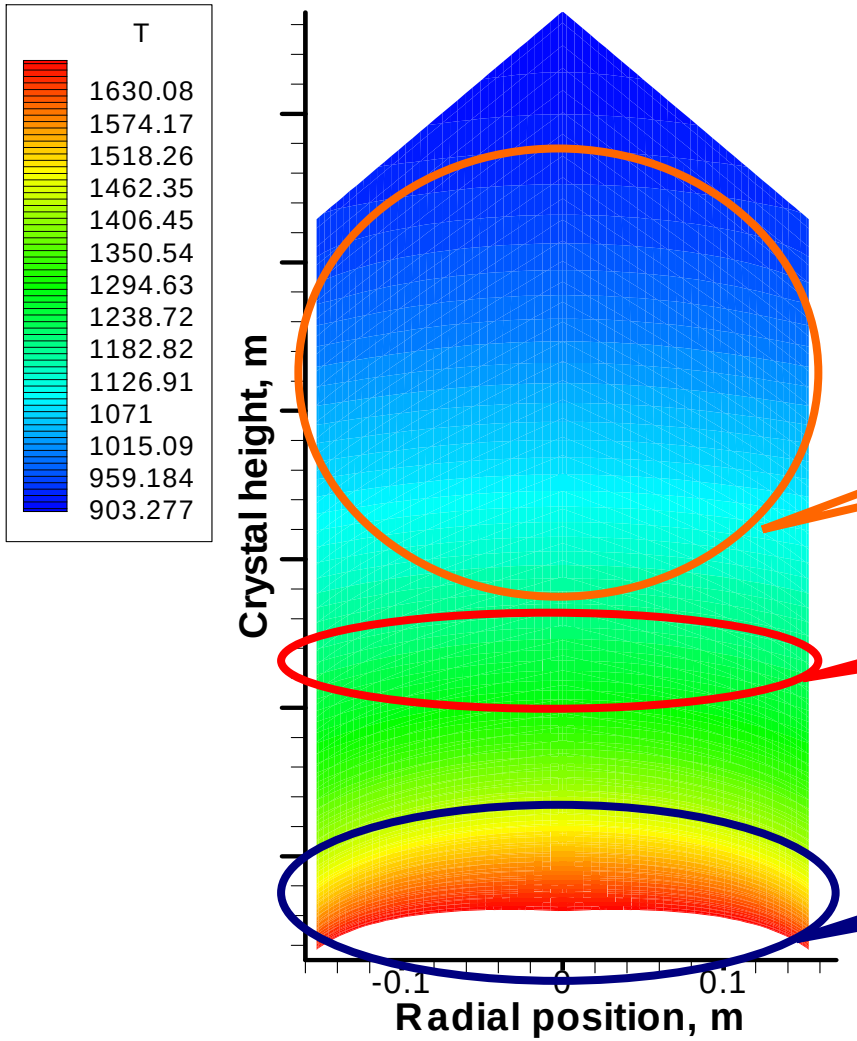

- *2D simulation of initial defects incorporation into the crystal.*
- *1D simulation of void and oxygen precipitate clusterization and evolution during crystal growth.*

Point defect growth region

Point defect nucleation region

Initial defect incorporation region

Initial defects incorporation governing equations

Initial defect kinetics:

$$\frac{\partial C_x}{\partial t} + \mathbf{V}\cdot\nabla C_x = \nabla\cdot\left(D_x(T)\nabla C_x\right) + K(T)\left(C_{ie}(T)C_{ve}(T) - C_i C_v\right)$$

x=v, i : vacancy and interstitial concentration respectively.

Convection term

Transient term

Fickian diffusion term

Recombination term

Recombination rate $K(T) = 4\pi a_r\left(D_i(T) + D_v(T)\right)\exp\left(-\frac{\Delta G}{kT}\right)$

Major physical features: *strong variation of defect equilibrium concentrations and diffusivities by the reason of the temperature distribution in the crystal and strong non-linear interdependence.*

Voronkov's approach: *fast recombination rate and corresponding quasi-equilibrium condition:* $C_{ie}(T)\cdot C_{ve}(T) = C_i \cdot C_v$

Brown's approach: *the system of coupled non-linear differential equations with standard recombination rate.*

The sensitivity of the results to the model input parameters

The heat and mass transfer model, coupled with melt convection models based on the 2D or the 3D assumptions produces different interface shapes and temperature fields affecting predicted incorporated initial defect concentrations.

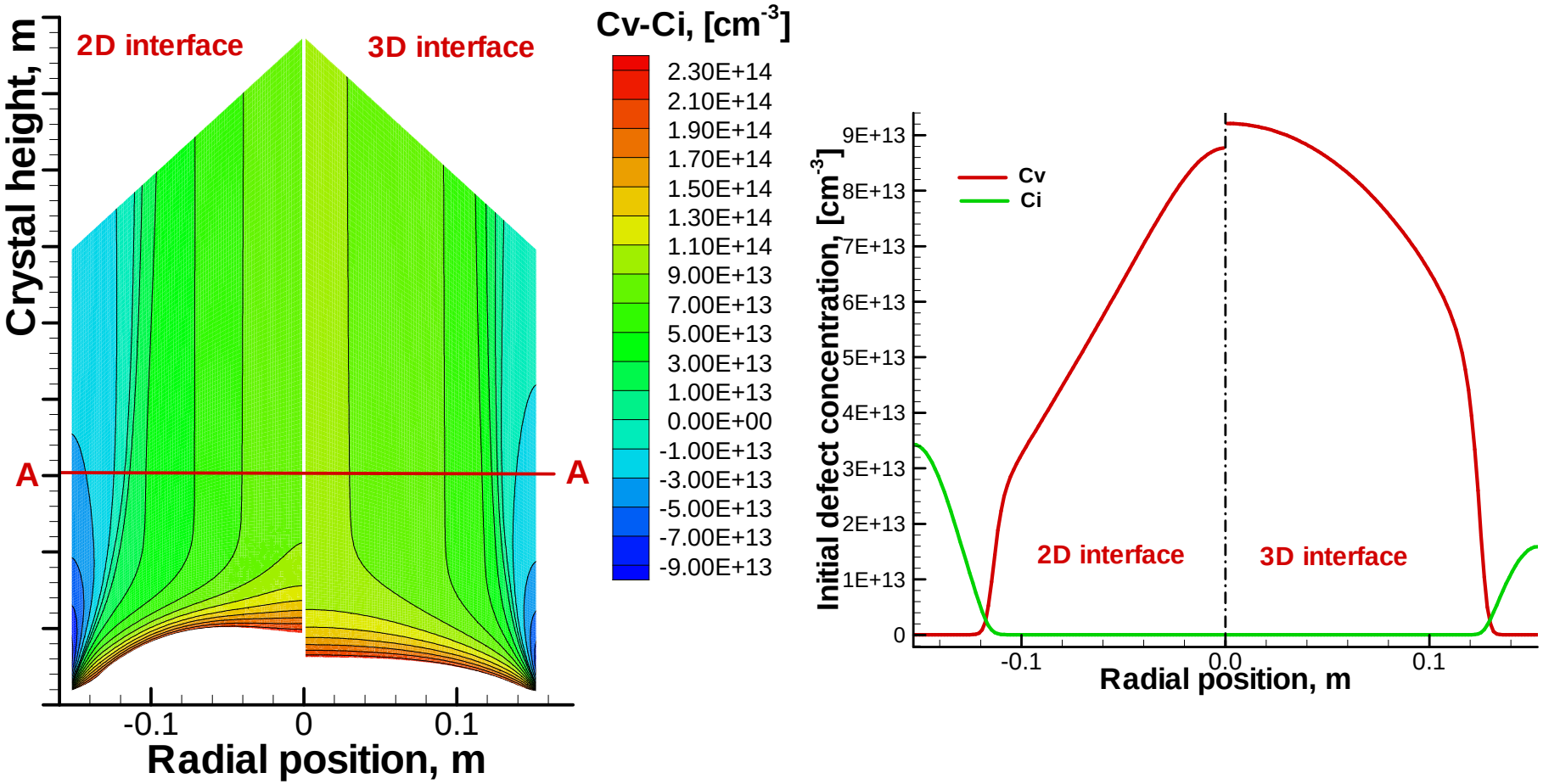

Spatial distributions and radial distributions for A-A cross-sections of initial defect concentration for the 300 mm diameter crystals with interfaces produced by the 2D and the 3D models.

The model of point defects nucleation and evolution

Basic physical model features and assumptions: *simultaneous nucleation and growth of voids and oxygen precipitates, multicomponent aggregations with kinetics which strongly depends on local temperature and initial defect concentration.*

The gain in the Gibbs free energy associated with void and oxygen precipitate formation depends on initial defect supersaturation and surface energy and can be written as

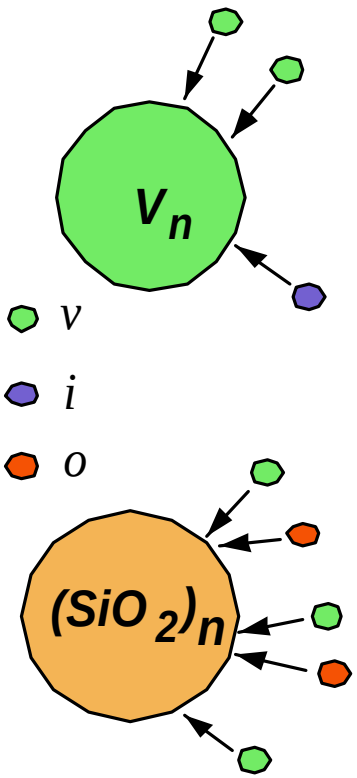

$$G_V = -\frac{4}{3}\pi R^3 \rho_V f_V + 4\pi^{2/3}\sqrt{3}\sigma_V R^2$$

$$G_P = -\frac{4}{3}\pi R^3 \rho_P f_P + 4\pi^{2/3}\sqrt{3}\sigma_P R^2$$

k=V,P : voids and oxygen precipitate respectively

R is a radius of the equivalent sphere

f_k is a volume free energy contribution

σ_k is an actual surface energy coefficient

ρ_k is atomic density associated with a point defect

Interstitial injection mechanism of stress energy relaxation for oxygen precipitate is neglected suppose high Frenkel pair formation energy, hence the stoichiometric condition for oxygen precipitate should be satisfied.

Simulation of void formation in a 300mm crystal

Variations in a crystal interface shape and corresponding temperature distribution can noticeable change radial distribution of void concentration and average size.

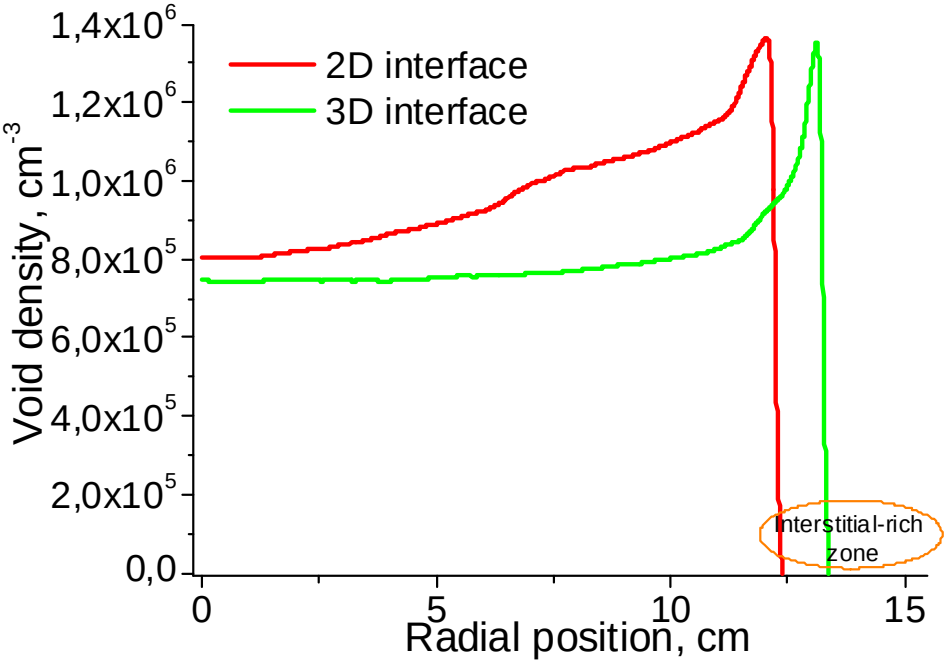

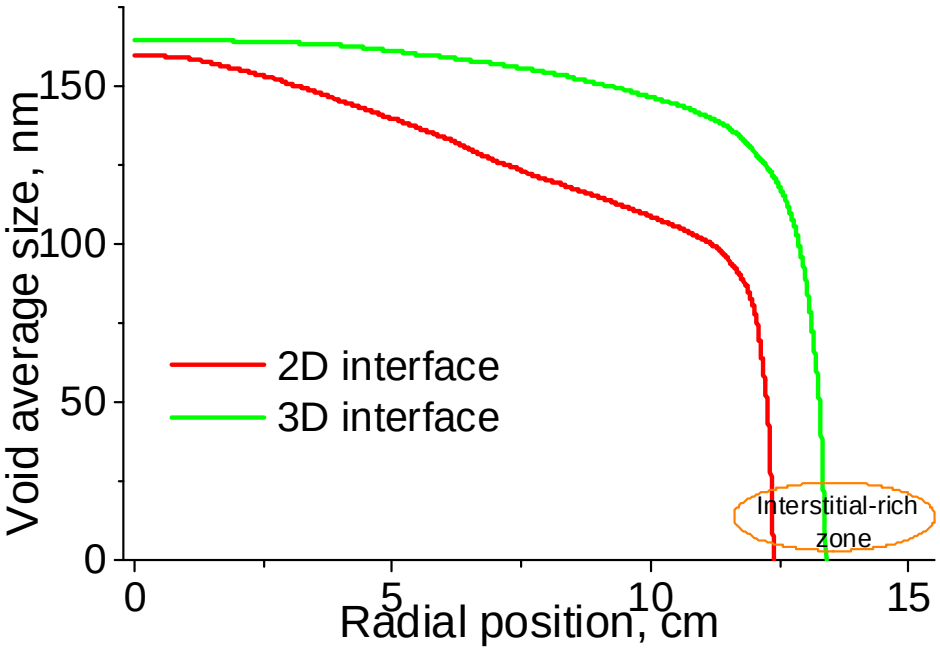

Average void size depends on incorporated vacancy concentration and correlates with total void density:
the higher point defect density, the less cluster size.

Simulation of oxygen precipitates formation

Variations in predicted initial defects concentrations can significantly affect predicted point defect concentrations and OSF-ring position in a crystal.

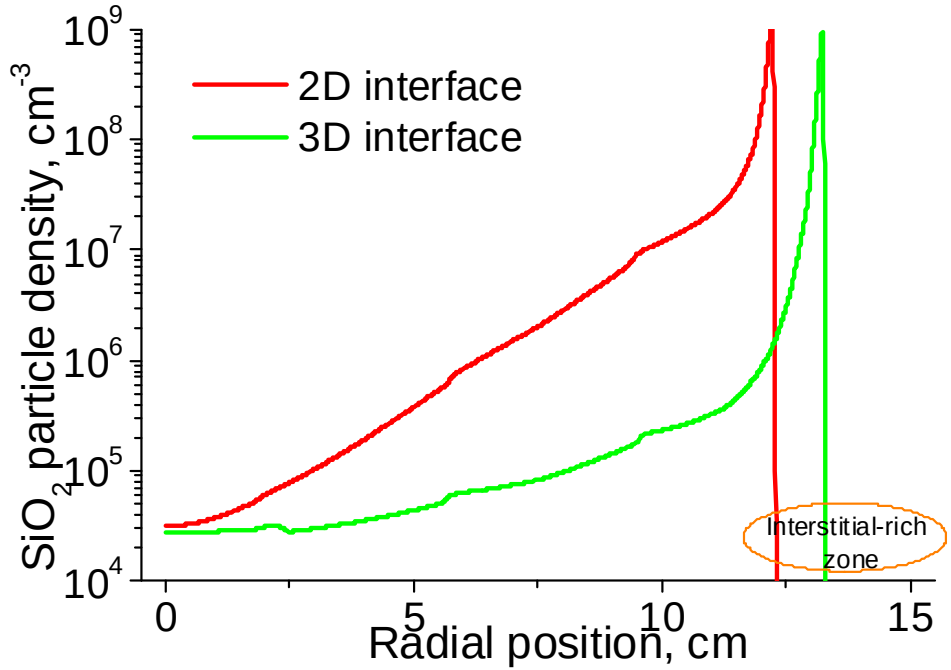

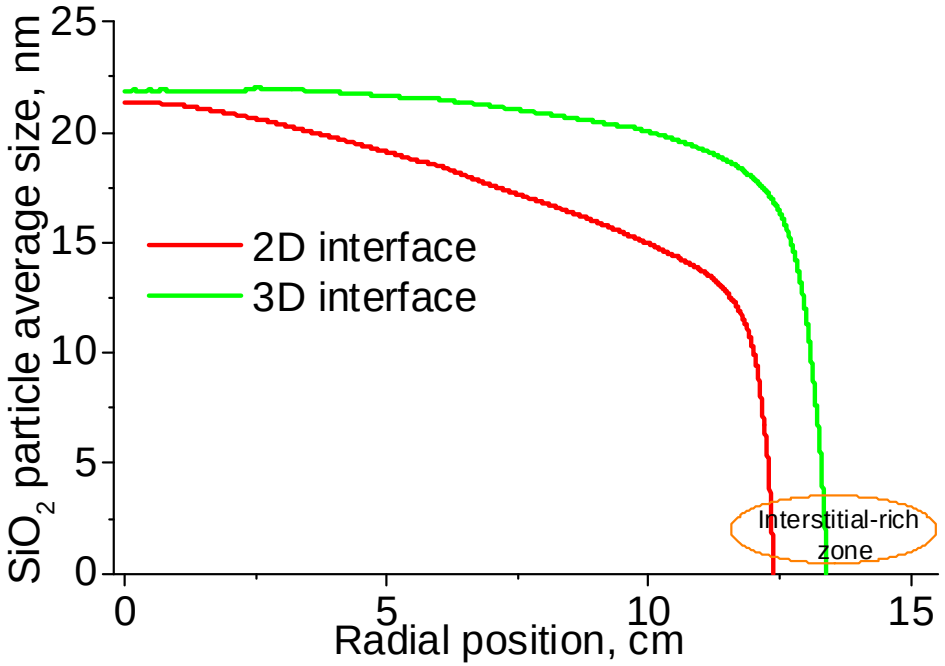

Radial distribution of oxygen precipitate average size shows the regularity which is similar to void's one: high point defect concentration in the OSF-ring corresponds with small oxygen precipitate size.

Summary

- *Temperature distribution in a growing crystal leads to high thermal stresses. Detailed numerical analysis is required to optimize the growth conditions.*
- *The model of initial defect incorporation considering vacancy and interstitial embedding at the melt/crystal interface and further transport into a crystal with simultaneous recombination has been developed.*
- *Predicted vacancy and interstitial concentration strongly depends on temperature distribution and used initial defect properties set.*
- *The physical model of point defect formation, which takes into account simultaneous nucleation and growth of voids and oxygen precipitates is presented.*
- *The strong dependence of point defect spatial distribution and average size on the interface shape and initial defect properties requires an adequate model of heat & mass transfer and reliable initial defect thermodynamic data.*

Thank you for the attention!